Physics of Fluids

Optic nerve microcirculation: Fluid flow and electrodiffusion

Cite as: Phys. Fluids **33**, 041906 (2021); https://doi.org/10.1063/5.0046323
Submitted: 02 February 2021 . Accepted: 05 April 2021 . Published Online: 30 April 2021

Yi Zhu (朱毅), Shixin Xu (徐士鑫), Robert S. Eisenberg, and Huaxiong Huang (黄华雄)

Physics of Fluids ARTICLE scitation.org/journal/phf

Optic nerve microcirculation: Fluid flow and electrodiffusion

Cite as: Phys. Fluids **33**, 041906 (2021); doi: 10.1063/5.0046323
Submitted: 2 February 2021 · Accepted: 5 April 2021 ·
Published Online: 30 April 2021

Yi Zhu (朱毅),[1] Shixin Xu (徐士鑫),[2,a)] Robert S. Eisenberg,[3,4] and Huaxiong Huang (黄华雄)[1,5,6,a)]

AFFILIATIONS

[1]Department of Mathematics and Statistics, York University, Toronto, Ontario M3J 1P3, Canada
[2]Zu Chongzhi Center for Mathematics and Computational Sciences, Division of Natural and Applied Sciences, Duke Kunshan University, 8 Duke Ave., Kunshan, Jiangsu 215316, China
[3]Department of Applied Mathematics, Illinois Institute of Technology, Chicago, Illinois 60616, USA
[4]Department of Physiology and Biophysics, Rush University, Chicago, Illinois 60612, USA
[5]Research Centre for Mathematics, Advanced Institute of Natural Sciences, Beijing Normal University, Zhuhai 519087, China
[6]Division of Science and Technology, BNU–HKBU United International College, Zhuhai 519087, China

[a)]**Authors to whom correspondence should be addressed:** shixin.xu@dukekunshan.edu.cn and hhuang@uic.edu.cn

ABSTRACT

Complex fluids flow in complex ways in complex structures. Transport of water and various organic and inorganic molecules in the central nervous system (CNS) are important in a wide range of biological and medical processes [C. Nicholson and S. Hrabětová, "Brain extracellular space: The final frontier of neuroscience," Biophys. J. **113**(10), 2133 (2017)]. However, the exact driving mechanisms are often not known. In this paper, we investigate flows induced by action potentials in an optic nerve as a prototype of the CNS. Different from traditional fluid dynamics problems, flows in biological tissues such as the CNS are coupled with ion transport. It is driven by osmosis created by the concentration gradient of ionic solutions, which in turn influence the transport of ions. Our mathematical model is based on the known structural and biophysical properties of the experimental system used by the Harvard group [R. K. Orkand, J. G. Nicholls, and S. W. Kuffler, "Effect of nerve impulses on the membrane potential of glial cells in the central nervous system of amphibia," J. Neurophysiol. **29**(4), 788 (1966)]. Asymptotic analysis and numerical computation show the significant role of water in convective ion transport. The full model (including water) and the electrodiffusion model (excluding water) are compared in detail to reveal an interesting interplay between water and ion transport. In the full model, convection due to water flow dominates inside the glial domain. This water flow in the glia contributes significantly to the spatial buffering of potassium in the extracellular space. Convection in the extracellular domain does not contribute significantly to spatial buffering. Electrodiffusion is the dominant mechanism for flows confined to the extracellular domain.

I. INTRODUCTION

The theory of complex fluids deals with complex fluids in complex structures.[1–4] Here, we deal with the complex fluid of an ionic solution[5] in a complex structure typical of biological systems in particular, the central nervous system (CNS). These structures are known in some detail—both structure and function—because of the work of generations of neuroanatomists, histologists, and neurobiologists.[6,7] The biophysical properties of membranes are also well known.[8] So we can formulate a biologically significant problem in the language of theory of complex fluids and use the methods of computational fluid mechanics to analyze the system, here the optic nerve of an amphibian. The results are of interest biologically because of the importance of the central nervous system: the optic nerve of amphibian is an experimentally accessible part of the central nervous system.

The analysis used here may also serve as a bridge and archetype of how the theory of complex fluids can deal with what at first may seem formidable challenges of structured biological systems in other biological systems, e.g., kidney, blood–brain barrier, and epithelial in general.

This paper is organized as follows: In Sec. II, we present the biological background of the optic nerve and the tridomain mathematical model in detail. The three domains, axon, glial and extracellular ones, are coupled via transmembrane fluxes for three major ions, namely sodium, potassium, and chloride, treated as reaction terms. Model

calibration is discussed in Sec. III by matching extracellular potassium concentration accumulation after the optic nerve is stimulated by a train of electric current pulses. In Sec. IV, we present estimates using order of magnitude analysis of transport of ionic and water fluxes cross membranes. They provide useful insight into the mechanisms for potassium clearance. Then in Sec. V, numerical simulations are carried out. We investigate the role of water flow (convection) in ionic transport during and after the stimulus of the optic nerve. Our analysis shows that convection is very important within the glia. Water flow in glia has an indirect but significant effect in clearing potassium from the narrow extracellular space. This may be an important role for glia wherever they are found in the central nervous system, and even in structures of the peripheral nervous system. A discussion on the parameters in the compartment models and field models are presented in Sec. VI. In Sec. VII, we provide concluding remarks on the limitation of our study and directions for future research.

II. BIOLOGICAL BACKGROUND AND MODEL

A. Biological background

Recent experimental studies[9] suggest that transport in the central nervous system during sleep plays a critical role in maintaining the health of brain tissue. Since the nervous system is densely packed with neurons communicating with each other, question arises: how is the state of steady internal conditions—known as "homeostasis" in the biological literature—maintained. A few action potentials are known to significantly alter ion concentration in the immediate vicinity of peripheral and optic nerve cells[10,11] and that change in concentration acts on more than one axon, producing "crosstalk." The question is then how does the central nervous system deal with changes in ion concentration produced by hundreds or thousands of action potentials and maintain a healthy environment? How does the central nervous system maintain concentrations in its narrow extracellular space? What are the roles played by of glial cells and extracellular space?

Complex flows in complex structures cannot be understood unless the structure is understood. The central nervous system contains nerve fibers and glia, separated by a narrow extracellular space. We use three domains to describe the flow and diffusion of ions and water in the optic nerve bundle of the central nervous system, hoping to glimpse general properties by which the central nervous system controls the concentration of ions in such narrow confines. The optic nerve bundle contains paired cranial nerve bundled with cell bodies in the retina. It reaches from the eye through the optic chiasma to the cortex and transfers visual information from the retina to the vision centers of the brain using digital (actually binary) electrical signals (action potentials). The optic nerve is customarily separated into four main regions:[12,13] (1) intraocular nerve head, (2) intraorbital region, (3) intracanalicular, and (4) intracranial.[12,14] In this paper, we mainly focus on the intraorbital region, which occupies more than half of the optic nerve.

There are about one million optic nerve fibers in the optic nerve bundle. The ganglion cells that are the cell bodies of the axons are scattered on the retina and form into a bundle at the optic disk. The bundle passes through the mesh-like lamina cribrosa region into the intraorbital region. Like almost all nerve cells, optic nerve fibers are functionally isolated, nearly insulated one from another, without connexins between them, so neither ions nor electrolytes can flow directly from the interior of one nerve cell to another. Current flow down one axon cannot flow into the adjacent axon or glia.[15,16] The "ephaptic communication" of concern to pioneers in electrophysiology rare occurs.

Glial cells wrap the nerve fiber bundles producing a narrow cleft of extracellular space between nerve fiber and glia. Glial cells are connected to each other through connexin proteins, called "gap junctions," and form an electrical syncytium (as do so many other cells, e.g., epithelia, cardiac muscle, lens of the eye, liver, etc.) in which current flow in one cell spreads into another with little extra resistance. In syncytia like this, inorganic ions, and many organic molecules (typically less than 2 nm diameter) can diffuse from cell to cell with hardly any restriction and thus with mobility and ionic conductance similar to that in cytoplasm. Thus, glial cells are thought to play an important role in accelerating K^+ clearance from the extracellular space.[17,18] Sometimes, central retinal blood vessels (CRVs, arterioles in fact) are found in the center of the optic nerve bundle in the intraorbital region. Here we consider the case where the blood vessel is not present, as in the optic nerve of the mud puppy, the amphibian salamander Necturus used in the experiments of Orkand *et al.*[10,16]

The optic nerve bundles are surrounded by the meningeal sheath which consists of dura mater, arachnoid mater, pia mater, and cerebrospinal fluid (CSF) in the subarachnoid space (SAS)[14,19] [also, see Fig. 1(a)]. The pia mater and dura mater are thin deformable shells, with mechanical properties important in glaucoma.[19–22] Andrew *et al.*[23] and Killer *et al.*[20,24] show that the dura mater contains lymphatic vessels that drain CSF out of SAS.[22,25] Pia mater forms a macroscopic semipermeable membrane made of many cells, not just one lipid bilayer.[26] Many layered epithelia have been characterized as "semipermeable membranes" in low-resolution studies of epithelia for more than a century. Filipidis *et al.*[27] have written a most helpful review that identifies analogous leptomeningeal structures important in the physiology of "like pleura,[28–33] peritoneum,[34–39] pericardium,[27] fetal membranes,[40,41] and leptomeninges,"[42] We imagine that a general tridomain model may help understand many of these tissues.

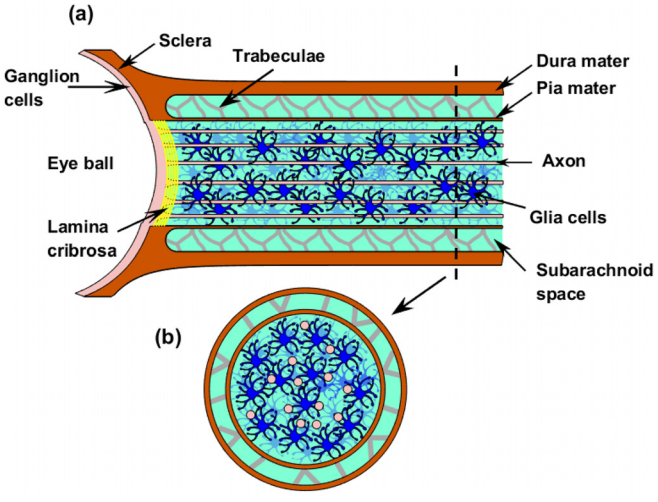

FIG. 1. Optic nerve structure: (a) longitudinal section of the optic nerve and (b) cross section of the optic nerve.

B. Mathematical model

The model is first proposed in Ref. 43. Here in order to make this paper self-contained, we summarize the model. The model deals with two types of flow: the circulation of water (hydrodynamics) and the circulation of ions (electrodynamics) in the glial compartment Ω_{gl}, axon compartment Ω_{ax} and extracellular space Ω_{ex}.

The glial compartment and axon compartment are limited to the optic nerve bundle, while extracellular space exists both in the optic nerve bundle Ω_{ex}^{OP} and in the subarachnoid space Ω_{ex}^{SAS} (see Fig. 2),

$$\Omega_{OP} = \Omega_{ax} \cup \Omega_{gl} \cup \Omega_{ex}^{OP}, \quad \Omega_{SAS} = \Omega_{ex}^{SAS}.$$

The model is mainly based on the law of mass conservation,[44] in Ω_l, $l = ax, gl, ex$

$$\frac{\partial}{\partial t}(\eta_l f_l) + \nabla \cdot (\eta_l \mathbf{J}_l) + S = 0, \tag{1}$$

where η_l is the volume fraction of l compartment, f_l is the concentration of given substance, $\mathbf{J}_l$ is the flux inside compartment, and S is the source term induced by the pumps and channels on the membranes.

We first introduce the following notations used in the paper, where $i = Na^+, K^+, Cl^-$ for ion species, $l = ex, gl, ax$ for extracellular space, glial compartment, and axon compartment, and $k = gl, ax$ for glial or axon membrane in the optic nerve. The summary of notations is listed in the Nomenclature.

In each domain, we assume electroneutrality such that

$$\eta_{gl} \sum_i z^i c_{gl}^i + z^{gl} \eta_{gl}^{re} A_{gl} = 0, \tag{2a}$$

$$\eta_{ax} \sum_i z^i c_{ax}^i + z^{ax} \eta_{ax}^{re} A_{ax} = 0, \tag{2b}$$

$$\sum_i z^i c_{ex}^i = 0, \tag{2c}$$

where $A_l > 0$ with $l = ax, gl$ is the density of proteins in axons or glial cells with valence z^l, $l = gl, ax$. The η_{ax} and η_{gl} are the volume fraction of axon and glial compartments in the optic nerve and η_{ax}^{re} and η_{gl}^{re} are the resting state volume fractions.

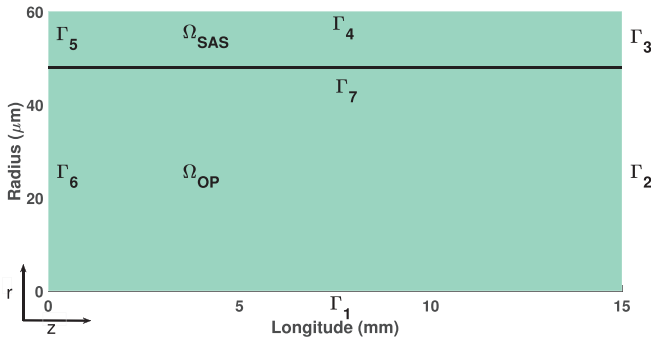

FIG. 2. Domain of axial symmetry model. The optic nerve Ω_{OP} consist of axon compartment Ω_{ax}, glial compartment Ω_{gl} and extracellular space Ω_{ex}^{OP}. The subarachnoid space Ω_{SAS} only has extracellular space.

1. Water circulation

The conservation of mass in each domain yields

$$\frac{\partial \eta_{gl}}{\partial t} + \mathscr{M}_{gl} U_{gl}^m + \nabla \cdot (\eta_{gl} \mathbf{u}_{gl}) = 0, \quad \text{in } \Omega_{OP}, \tag{3a}$$

$$\frac{\partial \eta_{ax}}{\partial t} + \mathscr{M}_{ax} U_{ax}^m + \frac{\partial}{\partial z}(\eta_{ax} u_{ax}^z) = 0, \quad \text{in } \Omega_{OP}, \tag{3b}$$

$$\nabla \cdot (\eta_{gl} \mathbf{u}_{gl}) + \nabla \cdot (\eta_{ex} \mathbf{u}_{ex}) + \frac{\partial}{\partial z}(\eta_{ax} u_{ax}^z) = 0, \quad \text{in } \Omega_{OP}, \tag{3c}$$

$$\eta_{gl} + \eta_{ax} + \eta_{ex} = 1, \quad \text{in } \Omega, \tag{3d}$$

where the transmembrane water flux is proportional to the intracellular/extracellular hydrostatic pressure and osmotic pressure differences, i.e., Starling's law on the membrane,

$$U_{gl}^m = L_{gl}^m (p_{gl} - p_{ex} - \gamma_{gl} k_B T (O_{gl} - O_{ex})),$$
$$U_{ax}^m = L_{ax}^m (p_{ax} - p_{ex} - \gamma_{ax} k_B T (O_{ax} - O_{ex})).$$

The glial cells are connected to each other by connexins and form a syncytium, while the axons are separate, more or less parallel cylindrical cells that do not form a syncytium (see Fig. 1). Then, we assume that glial cells are isotropic and axons are anisotropic. Here, $\mathbf{u}_l$ and p_l with $l = gl, ax, ex$ are the velocity and pressure in the glial cells and axons and extracellular space, respectively. $k_B T O_l$ is the osmotic pressure[45,46] defined by

$$O_{ex} = \sum_i c_{ex}^i, \quad O_l = \sum_i c_l^i + A_l \frac{\eta_j^{re}}{\eta_l}, \quad l = gl, ax,$$

where $A_l \frac{\eta_l^{re}}{\eta_l} > 0$ $(l = gl, ax)$ is the density of the permanent negatively charged protein in glial cell and axons that vary with the volume (fraction) of the region.

The relation between the hydrostatic pressure p_l and volume fraction η_l $(l = ex, gl, ax)$ is connected by the force balance on the membrane $k(= gl, ax)$,[45,47]

$$K_{gl}(\eta_{gl} - \eta_{gl}^{re}) = p_{gl} - p_{ex} - (p_{gl}^{re} - p_{ex}^{re}), \quad \text{in } \Omega_{OP}, \tag{4a}$$

$$K_{ax}(\eta_{ax} - \eta_{ax}^{re}) = p_{ax} - p_{ex} - (p_{ax}^{re} - p_{ex}^{re}), \quad \text{in } \Omega_{OP}, \tag{4b}$$

where K_k $(k = gl, ax)$ is the stiffness constant related to Young's modules and Poisson's ratio. The p_l^{re} $(l = gl, ax, ex)$ is the resting state hydrostatic pressure.

Remark 1. If we introduce the characteristic velocities u_l^* in l compartment, the characteristic transmembrane velocity U_l^*, the characteristic time t^*, the characteristic lengths r^* in radius direction and z^* in longitude direction, Eqs. (3a)–(3c) could be written as

$$\frac{\partial \eta_{gl}}{\partial \tilde{t}} + \delta_1 \tilde{U}_{gl}^m + \delta_2 \tilde{\nabla} \cdot (\eta_{gl} \tilde{\mathbf{u}}_{gl}) = 0, \tag{5a}$$

$$\frac{\partial \eta_{ax}}{\partial \tilde{t}} + \delta_3 \tilde{U}_{ax}^m + \delta_4 \frac{\partial (\eta_{ax} \tilde{u}_{ax}^z)}{\partial \tilde{z}} = 0, \tag{5b}$$

$$\tilde{\nabla} \cdot (\eta_{ex} \tilde{\mathbf{u}}_{ex}) + \delta_5 \tilde{\nabla} \cdot (\eta_{gl} \tilde{\mathbf{u}}_{gl}) + \delta_6 \delta_0 \frac{\partial (\eta_{ax} \tilde{u}_{ax}^z)}{\partial \tilde{z}} = 0, \tag{5c}$$

where

$$\tilde{\nabla}\cdot(\eta_l\tilde{\mathbf{u}}_l)=\frac{1}{\tilde{r}}\frac{\partial(\tilde{r}\eta_l\tilde{u}_l^r)}{\partial\tilde{r}}+\delta_0\frac{\partial(\eta_l\tilde{u}_l^z)}{\partial\tilde{z}},\quad l=gl,ex,$$

and

$$\delta_0=\frac{r^*}{z^*},\quad \delta_1=\mathscr{M}_{gl}U_{gl}^*t^*,\quad \delta_2=\frac{u_{gl}^*t^*}{r^*},\quad \delta_3=\mathscr{M}_{ax}U_{ax}^*t^*,$$
$$\delta_4=\frac{u_{ax}^*t^*}{z^*},\quad \delta_5=\frac{u_{gl}^*}{u_{ex}^*},\quad \delta_6=\frac{u_{ax}^*}{u_{ex}^*}.$$

Further scaling can be applied for velocity components in the r and z directions when the cross membrane flux is absent due to incompressibility. However, no such scaling is considered due to significant cross membrane flux.

The water flows in glial, axon compartments, and extracellular space are low Reynold number flows and the characteristic velocity is around 1–10 nm/s due to the existence of connexin and high tortuosity. Then the stationary Stokes equation is used

$$-\nabla\cdot(\mu\nabla\boldsymbol{u}_l)+\nabla p_l=f_l,$$

where f_l is the body force density in different compartments, for example, Lorentz force in the extracellular space.[48] Next, since the tissues have similar property as the porous media, The rigorous homogenization theories[49,50] or the control volume average methods[51,52] yield Darcy's law is a good macro-scale approximation for the Stokes flow in the porous media. For the sake of simplicity, we model flows in the following as porous media flows by using Darcy's law.[46,47]

a. Fluid velocity in the glial compartment. As we mentioned before, the glial space is a connected space, where water can flow from cell to cell through connexin proteins joining membranes of neighboring cells.

The velocity of fluid in glial syncytium $\mathbf{u}_{gl}$ depends on the gradients of hydrostatic pressure and osmotic pressure,

$$u_{gl}^r=-\frac{\kappa_{gl}\tau_{gl}}{\mu}\left(\frac{\partial p_{gl}}{\partial r}-\gamma_{gl}k_BT\frac{\partial O_{gl}}{\partial r}\right),\tag{6a}$$

$$u_{gl}^z=-\frac{\kappa_{gl}\tau_{gl}}{\mu}\left(\frac{\partial p_{gl}}{\partial z}-\gamma_{gl}k_BT\frac{\partial O_{gl}}{\partial z}\right).\tag{6b}$$

The boundary conditions of fluid in the glial syncytium are as follows:

$$\begin{cases}\mathbf{u}_{gl}\cdot\hat{\mathbf{r}}=0, & \text{on } \Gamma_1,\\ \nabla p_{gl}\cdot\hat{\mathbf{z}}=0, & \text{on } \Gamma_2,\\ \nabla p_{gl}\cdot\hat{\mathbf{z}}=0, & \text{on } \Gamma_6,\\ \mathbf{u}_{gl}\cdot\hat{\mathbf{r}}=0, & \text{on } \Gamma_7.\end{cases}\tag{7}$$

b. Fluid velocity in the axon compartment. Since the axons are only connected in the longitudinal direction and the fluid velocity in the axon region is defined along the z-direction as

$$u_{ax}^r=0,\tag{8a}$$

$$u_{ax}^z=-\frac{\kappa_{ax}}{\mu}\frac{\partial p_{ax}}{\partial z}.\tag{8b}$$

Dirichlet boundary conditions are used to the fluid velocity in axons

$$\nabla p_{ax}\cdot\hat{\mathbf{z}}=0,\quad \text{on } \Gamma_2\cup\Gamma_6.\tag{9}$$

c. Fluid velocity in the extracellular space. The extracellular space is narrow, and the extracellular velocity is determined by the gradients of hydro-static pressure and electric potential,

$$u_{ex}^r=-\frac{\kappa_{ex}\tau_{ex}}{\mu}\frac{\partial p_{ex}}{\partial r}-k_e\tau_{ex}\frac{\partial\phi_{ex}}{\partial r},\tag{10a}$$

$$u_{ex}^z=-\frac{\kappa_{ex}\tau_{ex}}{\mu}\frac{\partial p_{ex}}{\partial z}-k_e\tau_{ex}\frac{\partial\phi_{ex}}{\partial z},\tag{10b}$$

where ϕ_{ex} is the electric potential in the extracellular space, τ_{ex} is the tortuosity of extracellular region[44,53] and μ is the viscosity of water, k_e is introduced to describe the effect of electro-osmotic flow,[54–56] κ_{ex} is the permeability of extracellular space. Here the hydro permeability κ_{ex}, tortuosity τ_{ex} and electric-osmotic parameter k_e have two distinguished values in the region Ω_{ex}^{OP} and Ω_{ex}^{SAS},

$$\kappa_{ex}=\begin{cases}\kappa_{ex}^{OP}, & \text{in } \Omega_{OP},\\ \kappa_{ex}^{SAS}, & \text{in } \Omega_{SAS},\end{cases}\quad \tau_{ex}=\begin{cases}\tau_{ex}^{OP}, & \text{in } \Omega_{OP},\\ \tau_{ex}^{SAS}, & \text{in } \Omega_{SAS},\end{cases}$$
$$k_e=\begin{cases}k_e^{OP}, & \text{in } \Omega_{OP},\\ k_e^{SAS}, & \text{in } \Omega_{SAS}.\end{cases}$$

Since $\Gamma_2\cup\Gamma_3$ are the far end of optic nerve away from eyeball and next to the optic canal, we assume the hydro-static pressure of extracellular is equal to the cerebrospinal fluid (CSF) pressure. On the other hand, the intraocular pressure (IOP) is imposed at Γ_6 where the extracellular space is connected to the retina. At boundary Γ_5, we assume a non-permeable boundary. We are aware of the significance of the pressures and flows at these boundaries for clinical phenomena including glaucoma[57–59] and will return to that subject in later publications.

The water flow across the semi-permeable membrane Γ_4 is produced by the lymphatic drainage on the dura membrane, which depends on the difference between extracellular pressure and orbital pressure (OBP). We assume the velocity across the pia membrane Γ_4, is continuous and determined by the combination of hydrostatic and osmotic pressures. To summarize, the boundary conditions of the extracellular fluid are

$$\begin{cases}\mathbf{u}_{ex}\cdot\hat{\mathbf{r}}=0, & \text{on } \Gamma_1,\\ p_{ex}=p_{CSF}, & \text{on } \Gamma_2\cup\Gamma_3,\\ \mathbf{u}_{ex}^{SAS}\cdot\hat{\mathbf{r}}=L_{dr}^m\left(p_{ex}^{SAS}-p_{OBP}\right), & \text{on } \Gamma_4,\\ \mathbf{u}_{ex}\cdot\hat{\mathbf{r}}=0, & \text{on } \Gamma_5,\\ p_{ex}=p_{ICP}, & \text{on } \Gamma_6,\\ \mathbf{u}_{ex}^{OP}\cdot\hat{\mathbf{r}}=\mathbf{u}_{ex}^{SAS}\cdot\hat{\mathbf{r}}\\ \qquad=L_{pia}^m\left(p_{ex}^{OP}-p_{ex}^{SAS}-\gamma_{pia}k_BT\left(O_{ex}^{OP}-O_{ex}^{SAS}\right)\right), & \text{on } \Gamma_7,\end{cases}\tag{11}$$

where p_{CSF} is the cerebrospinal fluid pressure[57] and p_{ICP} is the pressure in the eye and p_{OBP} is the orbital pressure on the dura mater.

Remark 2. *Substituting velocities (6), (8), and (10) into conservation law equation (3) yields Poisson equations of hydrostatic pressures in different compartments. Equations (6), (8), and (10) mean that velocities vary in both r- and z-direction, which depend on the gradient*

of the hydrostatic pressure, osmotic pressure, or electric field. The distribution of velocity in radius direction during and after a train of stimuli is shown in Appendix F, Fig. 17.

2. Ion transport

The conservation of chemical species implies the following system of partial differential equations to describe the dynamics of ions in each region, for $i = \mathrm{Na}^+, \mathrm{K}^+, \mathrm{Cl}^-$:

$$\frac{\partial\left(\eta_{gl}c^i_{gl}\right)}{\partial t} + \mathscr{M}_{gl}J^{m,i}_{gl} + \nabla\cdot\left(\eta_{gl}\mathbf{j}^i_{gl}\right) = 0, \quad \text{in } \Omega_{OP}, \tag{12}$$

$$\frac{\partial\left(\eta_{ax}c^i_{ax}\right)}{\partial t} + \mathscr{M}_{ax}J^{m,i}_{ax} + \frac{\partial}{\partial z}\left(\eta_{ax}j^i_{ax,z}\right) = 0, \quad \text{in } \Omega_{OP}, \tag{13}$$

$$\frac{\partial\left(\eta_{ex}c^i_{ex}\right)}{\partial t} - \mathscr{M}_{ax}J^{m,i}_{ax} - \mathscr{M}_{gl}J^{m,i}_{gl} + \nabla\cdot\left(\eta_{ex}\mathbf{j}^i_{ex}\right) = 0, \quad \text{in } \Omega_{OP}, \tag{14}$$

where the last equation reduces to the following in the Ω_{SAS} region:

$$\frac{\partial c^{i,SAS}_{ex}}{\partial t} + \nabla\cdot\mathbf{j}^{i,SAS}_{ex} = 0. \tag{15}$$

The transmembrane ion flux $J^{m,i}_k\,(k = gl, ax)$ consists of active ion pump source $J^i_{p,k}$ and passive ion channel source $J^i_{c,k}$, on the k membrane,

$$J^{m,i}_k = J^i_{p,k} + J^i_{c,k}, \quad k = gl, ax, \quad i = \mathrm{Na}^+, \mathrm{K}^+, \mathrm{Cl}^-.$$

On the glial cell membranes, $J^i_{c,gl}$ is defined as

$$J^i_{c,gl} = \frac{g^i_{gl}}{z^i e}\left(\phi_{gl} - \phi_{ex} - E^i_{gl}\right), \quad i = \mathrm{Na}^+, \mathrm{K}^+, \mathrm{Cl}^-, \tag{16}$$

where the Nernst potential is used to describe the gradient of chemical potential $E^i_{gl} = \frac{k_B T}{ez^i}\log\left(\frac{c^i_{ex}}{c^i_{gl}}\right)$ and the conductance g^i_{gl} for ith ion specie on the glial membrane is a fixed constant, independent of voltage and time. On the axon's membrane, $J^i_{c,ax}$ is defined as

$$J^i_{c,ax} = \frac{g^i_{ax}}{z^i e}\left(\phi_{ax} - \phi_{ex} - E^i_{ax}\right), \quad i = \mathrm{Na}^+, \mathrm{K}^+, \mathrm{Cl}^-,$$

where

$$g^{Na}_{ax} = \bar{g}^{Na}m^3h + g^{Na}_{leak}, \quad g^K_{ax} = \bar{g}^K n^4 + g^K_{leak}, \quad g^{Cl}_{ax} = g^{Cl}_{leak}.$$

The time-dependent dynamic of open probability, often loosely called "gating" is governed by the Hodgkin–Huxley model[60,61]

$$\begin{aligned}\frac{dn}{dt} &= \alpha_n(1-n) - \beta_n n,\\ \frac{dm}{dt} &= \alpha_m(1-m) - \beta_m m,\\ \frac{dh}{dt} &= \alpha_h(1-h) - \beta_h h,\end{aligned} \tag{17}$$

where n is the open probability of K^+ channel, m is the open probability of the Na^+ activation gate, and h is the open probability of the Na^+ inactivation gate.

We assume that the only pump is the Na/K active transporter. We are more than aware that other active transport systems can and likely do move ions and thus water in this system. They will be included as experimental information becomes available.

In the case of the Na/K pump $J^i_{p,k}\ (k = ax, gl)$, the strength of the pump I_k depends on the concentration in the intracellular and extracellular space,[60,62] i.e.,

$$J^{Na}_{p,k} = \frac{3I_k}{e}, \quad J^K_{p,k} = -\frac{2I_k}{e}, \quad J^{Cl}_{p,k} = 0, \quad k = gl, ax, \tag{18}$$

where

$$\begin{aligned}I_k = I_{k,1}&\left(\frac{c^{Na}_k}{c^{Na}_k + K_{Na1}}\right)^3\left(\frac{c^K_{ex}}{c^K_{ex} + K_{K1}}\right)^2\\ &+ I_{k,2}\left(\frac{c^{Na}_k}{c^{Na}_k + K_{Na2}}\right)^3\left(\frac{c^K_{ex}}{c^K_{ex} + K_{K2}}\right)^2, \quad k = ax, gl.\end{aligned} \tag{19}$$

$I_{k,1}$ and $I_{k,2}$ are related to the maximum current of α_1- and α_2- isoform of Na/K pump on the glial membrane ($k = gl$) or axon membrane ($k = ax$).

The definitions of ion flux in each domain are as follows, for $i = \mathrm{Na}^+, \mathrm{K}^+, \mathrm{Cl}^-$:

$$\mathbf{j}^i_l = c^i_l\mathbf{u}_l - D^i_l\tau_l\left(\nabla c^i_l + \frac{z^i e}{k_B T}c^i_l\nabla\phi_l\right), \quad l = gl, ex,$$

$$j^i_{ax,z} = c^i_{ax}u^z_{ax} - D^i_{ax}\left(\frac{\partial c^i_{ax}}{\partial z} + \frac{z^i e}{k_B T}c^i_{ax}\frac{\partial\phi_{ax}}{\partial z}\right).$$

For the axon compartment and glial compartment boundary condition, we have

$$c^i_{ax} = c^{i,re}_{ax}, \quad \text{on } \Gamma_2\cup\Gamma_6, \tag{20}$$

and

$$\begin{cases}\mathbf{j}^i_{gl}\cdot\hat{\mathbf{r}} = 0, & \text{on } \Gamma_1,\\ c^i_{gl} = c^{i,re}_{gl}, & \text{on } \Gamma_2\cup\Gamma_6,\\ \mathbf{j}^i_{gl}\cdot\hat{\mathbf{r}} = 0, & \text{on } \Gamma_7,\end{cases} \tag{21}$$

where the Dirichlet boundary conditions are used at locations $\Gamma_2\cup\Gamma_6$ for axons and glial cell, and a non-flux boundary condition is used for glial cells ions flux on pia mater Γ_7.

For the extracellular space boundary condition, similar boundary conditions are imposed except on the pia mater Γ_7. The flux across the pia mater is assumed continuous and Ohm's law is used.[46] Additionally, a non-permeable boundary condition is used at location Γ_5 and a homogeneous Neumann boundary condition is applied at the location of the dura mater Γ_4,

$$\begin{cases}\mathbf{j}^i_{ex}\cdot\hat{\mathbf{r}} = 0, & \text{on } \Gamma_1,\\ c^i_{ex} = c^i_{csf}, & \text{on } \Gamma_2\cup\Gamma_3,\\ \nabla c^i_{ex}\cdot\hat{\mathbf{r}} = 0, & \text{on } \Gamma_4,\\ \mathbf{j}^i_{ex}\cdot\hat{\mathbf{z}} = 0, & \text{on } \Gamma_5,\\ c^i_{ex} = c^i_{eye}, & \text{on } \Gamma_6,\\ \mathbf{j}^{i,OP}_{ex}\cdot\hat{\mathbf{r}} = \mathbf{j}^{i,SAS}_{ex}\cdot\hat{\mathbf{r}} = \dfrac{G^i_{pia}}{z^i e}\left(\phi^{OP}_{ex} - \phi^{SAS}_{ex} - E^i_{pia}\right), & \text{on } \Gamma_7.\end{cases} \tag{22}$$

Remark 3. Suppose the $c_l^{i,*}$ is the scale of i ion specie in the l space and $\Delta c_l^{i,*}$ is the scale of r and th$z$-direction i ion specie concentration variation in the l space. If we define

$$\delta_{7,l}^i = \frac{\Delta c_l^{i,*}}{c_l^{i,*}}, \quad i = \mathrm{Na}^+, \mathrm{K}^+, \mathrm{Cl}^+, \quad l = ax, gl, ex.$$

The ion fluxes could be written as

$$\tilde{\mathbf{j}}_l^i = Pe_l^i \delta_{7,l}^i \tilde{c}_l^i \tilde{\mathbf{u}}_l - \left(\delta_{7,l}^i \tilde{\nabla} \tilde{c}_l^i + z^i \tilde{c}_l^i \tilde{\nabla} \tilde{\phi}_l\right), \quad l = gl, ex,$$

$$\tilde{j}_{ax,z}^i = Pe_{ax}^i \delta_{7,l}^i \tilde{c}_l^i \tilde{u}_{ax}^z - \left(\delta_{7,l}^i \frac{\partial \tilde{c}_l^i}{\partial \tilde{z}} + z^i \tilde{c}_l^i \frac{\partial \tilde{\phi}_l}{\partial \tilde{z}}\right),$$

with Peclet numbers

$$Pe_{ax}^i = \frac{u_{ax}^* z^* c_{ax}^{i,*}}{D_{ax}^i \Delta c_{ax}^{i,*}}, \quad Pe_l^i = \frac{u_l^* r^* c_l^{i,*}}{D_l^i \tau_l \Delta c_l^{i,*}}, \quad l = gl, ex. \tag{23}$$

If we let g_l^*, $l = ax, gl$ be the characteristic membrane conductance, $\frac{k_B T}{e}$ be the characteristic electric potential, the dimensionless form of transmembrance flux is

$$\tilde{J}_l^{m,i} = \tilde{J}_{c,l}^i + \tilde{J}_{p,l}^i,$$

where for $i = \mathrm{Na}^+, \mathrm{K}^+, \mathrm{Cl}^-$, $l = gl, ax$,

$$\tilde{J}_{c,l}^i = \frac{\tilde{g}_l^i}{z^i}\left(\tilde{\phi}_k - \tilde{\phi}_{ex} - \tilde{E}_{gl}^i\right), \quad \tilde{J}_{p,l}^i = \frac{J_{p,l}^i e^2}{k_B T g_l^*}.$$

The governing equations for ions become

$$\frac{\partial\left(\eta_{gl}\tilde{c}_{gl}^i\right)}{\partial \tilde{t}} + \delta_8^i \tilde{J}_{gl}^{m,i} + \delta_9^i \tilde{\nabla} \cdot \left(\eta_{gl}\tilde{\mathbf{j}}_{gl}^i\right) = 0, \tag{24}$$

$$\frac{\partial\left(\eta_{ax}\tilde{c}_{ax}^i\right)}{\partial \tilde{t}} + \delta_{10}^i \tilde{J}_{ax}^{m,i} + \delta_{11}^i \frac{\partial}{\partial \tilde{z}}\left(\eta_{ax}\tilde{j}_{ax,z}^i\right) = 0, \tag{25}$$

$$\frac{\partial\left(\eta_{ex}\tilde{c}_{ex}^i\right)}{\partial \tilde{t}} - \delta_{12}^i \delta_{10}^i \tilde{J}_{ax}^{m,i} - \delta_{13}^i \delta_8^i \tilde{J}_{gl}^{m,i} + \delta_{14}^i \tilde{\nabla} \cdot \left(\eta_{ex}\tilde{\mathbf{j}}_{ex}^i\right) = 0, \tag{26}$$

where

$$\tilde{\nabla} \cdot \left(\eta_l \tilde{\mathbf{j}}_l^i\right) = \frac{1}{\tilde{r}} \frac{\partial\left(\tilde{r}\eta_l \tilde{j}_l^{r,i}\right)}{\partial \tilde{r}} + (\delta_0)^2 \frac{\partial\left(\eta_l \tilde{j}_l^{z,i}\right)}{\partial \tilde{z}}, \quad l = gl, ex,$$

$$\delta_8^i = \frac{t^* \mathscr{M}_{gl} g_{gl}^* k_B T}{c_{gl}^{i,*} e^2}, \quad \delta_9^i = \frac{D_{gl}^i \tau_{gl} t^*}{(r^*)^2},$$

$$\delta_{10}^i = \frac{t^* \mathscr{M}_{ax} g_{ax}^* k_B T}{c_{ax}^{i,*} e^2}, \quad \delta_{11}^i = \frac{D_{ax}^i t^*}{(z^*)^2},$$

$$\delta_{12}^i = \frac{c_{ax}^{i,*}}{c_{ex}^{i,*}}, \quad \delta_{13}^i = \frac{c_{gl}^{i,*}}{c_{ex}^{i,*}}, \quad \delta_{14}^i = \frac{D_{ex}^i \tau_{ex} t^*}{(r^*)^2}.$$

Remark 4. *In the rest of this paper, the symbol Δf is used to denote the variation of the variable f from its resting state value.*

Multiplying equations in (12)–(14) with $z_i e$, respectively, summing up, and using the charge neutrality condition, we have the following system for the electric fields in *ax*, *gl*, *ex*:

$$\sum_i z^i e \mathscr{M}_{gl} J_{gl}^{m,i} + \sum_i \nabla \cdot \left(z^i e \eta_g \mathbf{j}_{gl}^i\right) = 0, \tag{27}$$

$$\sum_i z^i e \mathscr{M}_{ax} J_{ax}^{m,i} + \sum_i \frac{\partial}{\partial z}\left(z^i e \eta_{ax} j_{ax,z}^i\right) = 0, \tag{28}$$

$$\sum_i z^i e \nabla \cdot \left(\eta_{gl}\mathbf{j}_{gl}^i\right) + \sum_i \frac{\partial}{\partial z}\left(z^i e \eta_{ax} j_{ax,z}^i\right) + \sum_i \nabla \cdot \left(z^i e \eta_{ex}\mathbf{j}_{ex}^i\right) = 0, \tag{29}$$

In the subarachnoid space Ω_{SAS}, the extracellular equations reduce to

$$\sum_i \nabla \cdot \left(z^i e \sum_i \mathbf{j}_{ex}^{i,SAS}\right) = 0. \tag{30}$$

The boundary conditions for electric fields ϕ_{ax}, ϕ_{gl} and ϕ_{ex} are given below.

In the axon compartment:

$$\begin{cases} \nabla \phi_{ax} \cdot \hat{\mathbf{z}} = 0, & \text{on } \Gamma_2, \\ \nabla \phi_{ax} \cdot \hat{\mathbf{z}} = 0, & \text{on } \Gamma_6, \end{cases} \tag{31}$$

In the glial compartment:

$$\begin{cases} \nabla \phi_{gl} \cdot \hat{\mathbf{r}} = 0, & \text{on } \Gamma_1, \\ \nabla \phi_{gl} \cdot \hat{\mathbf{z}} = 0, & \text{on } \Gamma_2, \\ \nabla \phi_{gl} \cdot \hat{\mathbf{z}} = 0, & \text{on } \Gamma_6, \\ \nabla \phi_{gl} \cdot \hat{\mathbf{r}} = 0, & \text{on } \Gamma_7, \end{cases} \tag{32}$$

and in the extracellular space:

$$\begin{cases} \nabla \phi_{ex} \cdot \hat{\mathbf{r}} = 0, & \text{on } \Gamma_1, \\ \nabla \phi_{ex} \cdot \hat{\mathbf{z}} = 0, & \text{on } \Gamma_2 \cup \Gamma_3, \\ \nabla \phi_{ex} \cdot \hat{\mathbf{r}} = 0, & \text{on } \Gamma_4, \\ \nabla \phi_{ex} \cdot \hat{\mathbf{z}} = 0, & \text{on } \Gamma_5, \\ \nabla \phi_{ex} \cdot \hat{\mathbf{z}} = 0, & \text{on } \Gamma_6, \\ \sum_i z^i e \mathbf{j}_{ex}^{i,OP} \cdot \hat{\mathbf{r}} = \sum_i z^i e \mathbf{j}_{ex}^{i,SAS} \cdot \hat{\mathbf{r}} & \\ \qquad = \sum_i G_{pia}^i \left(\phi_{ex}^{OP} - \phi_{ex}^{SAS} - E_{pia}^i\right), & \text{on } \Gamma_7. \end{cases} \tag{33}$$

In the rest of this paper, the full electric-diffusion-convection model is defined by Eqs. (3a)–(33). The electric-diffusion model is defined by Eqs. (12)–(33). The electric diffusion model is a reduced version of the full model in which water is neglected.

III. MODEL CALIBRATION AND VALIDATION

In this section, we use the physiological and anatomical data in Orkand *et al.*[10] to calibrate the value of parameters, like membrane conductance, capacitance, and structural parameters. We then validate our model by computing results with these parameters and comparing the computation with the experiment, which are designed to measure the change in potential across the glial membrane produced by a train of action potentials.

In the Orkand experiment, optic nerve has been put in bathing solutions with three different K^+ concentration (1.5, 3, 4.5 mM) and the resting potential across the glia membrane was measured. Then the axon was stimulated simultaneously at both ends (see lines 5–6 of

the Methods section of Orkand paper) to give a train of action potentials. The action potentials increased K^+ in extracellular space (ECS). The accumulated K^+ then made the glia membrane potential more positive.

In the simulation, we applied a train of stimuli with frequency $17/s$ for 1 s to the axon membrane at $z = 2.25, 13.5, 0 < r < R_a = 48\,\mu$m. Each individual stimulus in the train lasted 3 ms (as Orkand's paper indicated) and had strength $3\,mA/m^2$. The stimulus was large enough to exceed threshold and generate action potentials. We set the ECS K^+ to be 1.5, 3, or 4.5 mM and record the largest absolute value of the change in glial membrane potential in each case as in Fig. 4. This number is loosely called "the depolarization" in most laboratories. The blue symbols show experimental data, red ones are the simulations results of electrodiffusion model and the green ones are the full model. Figure 4 shows that both the full model and electrodiffusion model could match the experimental resting potentials (solid symbols) and depolarizations (open symbols) very well for the different ECS K^+ concentrations.

Figure 3 shows the propagation of the axon action potential. The membrane potential from axons at the center of the optic nerve bundle is shown when different locations of the axon had been stimulated. In both eye-end and two-end cases, the stimulus current was applied from $t = 1$ ms to $t = 4$ ms. In Fig. 3(a), the stimulus was applied near to the optic nerve near the eye-end ($z = 2.25$ mm). At $t = 1$ ms, the discontinuity of stimulus current induces jumps of the axon membrane potential in Fig. 3. At $t = 10$ ms, the action potential completely

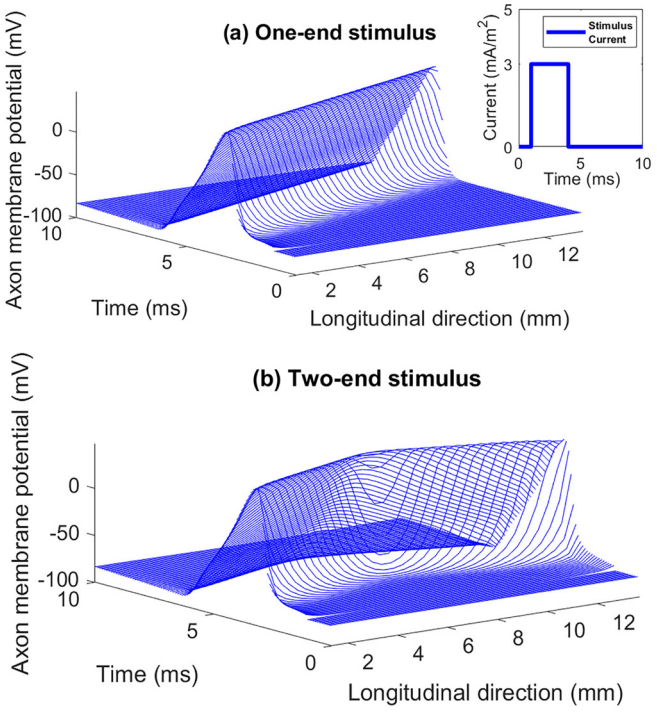

FIG. 3. (a) Axon membrane potential profile when eye-end axon stimulated. The built-in figure is the stimulus current profile. (b) Axon membrane potential profile when two-end axon simulated.

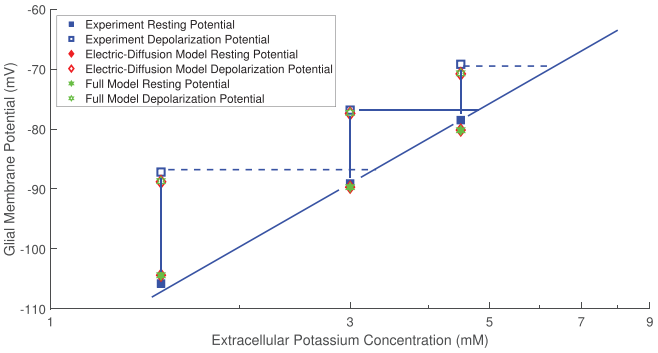

FIG. 4. The comparison between the experiment[10] and simulation on the effect of nerve impulses on the membrane potential of glial cells. The solid symbols are resting potentials and the open symbols are depolarization potentials with different ECS K^+ concentrations.

has propagated and left the location near far-eye-end (13.5 mm). The axon in the optic nerve of the mud puppy is unmyelinated. This speed of action potential propagation in the model lies in the range of the action potential speeds typical of unmyelinated axons, i.e., between $0.5\,m/s$ and $2.0\,m/s$.[63] In Fig. 3(b), when the two ends of the axon stimulated, the axon membrane potential has is more uniform spatially at each time point in comparison to the single side stimulus case. Orkand *et al.* used the dual stimulation to more closely approximate a "space clamp."

IV. EFFECTS OF WATER FLOW

In this section, when part of the nerve is stimulated, we estimate the transmembrane fluxes and the resulting accumulation of ions in the extracellular space and glial cells. Our main conclusion is that the variation of osmotic pressure between extracellular space and glial cells is the dominant mechanism that drives water flow, and water flows are significant and many important flows occur in the glial region. It is important to note that these flows can occur in the glia because it is a syncytium of irregular but finite cells (i.e., not long cylinders) that allows easy flow from cell to cell. The circulation pattern and strength of water flow in optic nerve are also presented.

To simplify our discussions, we focus our analyses on an idealized setting where the stimulus is applied at an inner part of the axon compartment. As shown in Fig. 5, the stimulus was applied at $0 < r < r_{sti}$ at a given location $z = z_0$. This stimulus is within the optic nerve, so $r_{sti} < R_a = r^*$ shown in Fig. 5. We distinguish the stimulated region and the nonstimulated region in the optic nerve Ω_{OP} shown in Fig. 5, since the electrical signal propagates in the z-direction in the axon compartment. We do not put the stimulus everywhere in this region, rather we only apply the stimulus at the location (z_0) within a radial.

To understand the mechanism inducing the water circulation, we first estimate the variations of ion concentrations from axon to the extracellular space during a single action potential. Then we analyze the different transmembrane current on the glial cells and identify the dominant K^+ current. Finally, we study osmotic pressure change after a train of action potentials on axon.

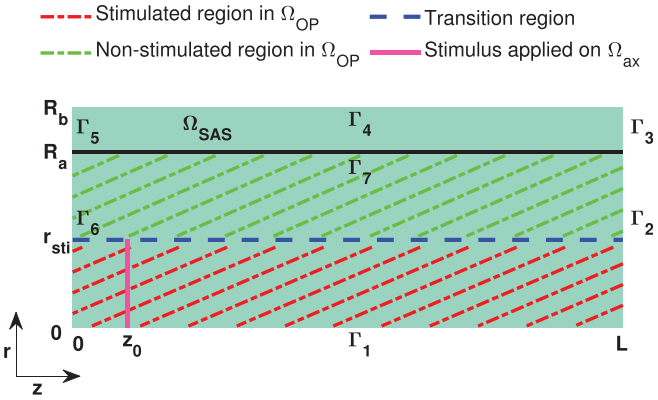

FIG. 5. Stimulated region and nonstimulated region in the optic nerve (Ω_{OP}). The stimulus is applied in the axon compartment where $0 < r < r_{sti}$ at a given location $z = z_0$.

A. Single action potential estimation

We first estimate the amount of ion exchange between axon and extracellular space during a single action potential. We assume that during the single action potential, the volume fraction η_l, $l = ax, gl, ex$, does not differ from their resting state. We find then that the variation of Na^+ and K^+ in the stimulated extracellular region is the same to leading order, and that agrees with experimental observations.[64–66] Although our estimation is based on the classic Hodgkin–Huxley model, the methods are general and can be applied to systems with other channels and transporters.

When an action potential occurs in the nerve, the equilibrium (or steady state) balance between the ions and electric fields is lost and resting state changes. We introduce notations to separate the resting state variables (with superscript "*re*") before the action potentials from the variables during the action potentials (with superscript "*dy*").

We introduce the current of *i*th ionic species through axon and glial membrane as

$$I_k^{i,j} = z^i e J_k^{m,i,j} = z^i e J_{p,k}^{i,j} + z^i e J_{c,k}^{i,j}, \quad i = \mathrm{Na}^+, \mathrm{K}^+, \mathrm{Cl}^-, \quad j = re, dy, \quad k = gl, ax,$$

where $J_k^{m,i,j}$ consists of the active Na/K pump source ($J_{p,k}^{i,j}$) and passive ion channel source ($J_{c,k}^{i,j}$) for *i*th ionic species on the axons ($k = ax$) or glial cells membranes ($k = gl$) at resting state ($j = re$) before the action potentials or during the action potentials ($j = dy$).

At the resting state, Na/K pump source $J_{p,k}^{i,re}$ and ion channels source $J_{c,k}^{i,re}$ on the axon membrane ($k = ax$) and glial membrane ($k = gl$) satisfy

$$J_{p,k}^{Na,re} = \frac{3I_k^{re}}{e}, \quad J_{p,k}^{K,re} = -\frac{2I_k^{re}}{e}, \quad J_{p,k}^{Cl,re} = 0,$$
$$J_{c,k}^{i,re} = \frac{g_k^{i,re}}{z^i e}\left(V_k^{re} - E_k^{i,re}\right), \quad i = \mathrm{Na}^+, \mathrm{K}^+, \mathrm{Cl}^-, \quad k = gl, ax$$

where the membrane potential V_k^{re} at the resting state is

$$V_k^{re} = \phi_k^{re} - \phi_{ex}^{re}, \quad k = gl, ax.$$

The ion channel conductance on the glial membrane is a fixed constant,

$$g_{gl}^{i,re} = g_{gl}^i, \quad i = \mathrm{Na}^+, \mathrm{K}^+, \mathrm{Cl}^-.$$

and the ion channel conductance on the axon membrane is defined as in the classical Hodgkin–Huxley model

$$g_{ax}^{Na,re} = \bar{g}^{Na}(m^{re})^3 h^{re} + g_{leak}^{Na}, \quad g_{ax}^{K,re} = \bar{g}^K (n^{re})^4 + g_{leak}^K, \quad g_{ax}^{Cl,re} = g_{leak}^{Cl},$$

The kinetic variables m^{re}, h^{re}, and n^{re} are measures of the resting state open probability for the voltage-gated Na^+ and K^+ channel on the axon membrane. In addition, in the resting state, the ion fluxes through the active Na/K pump $J_{p,k}^{i,re}$ and ion channel $J_{c,k}^{i,re}$ in the glial membrane ($k = gl$) or axon membrane ($k = ax$) are balanced in magnitude

$$O\left(|J_{p,k}^{i,re}|\right) = O\left(|J_{c,k}^{i,re}|\right), \quad i = \mathrm{Na}^+, \mathrm{K}^+, \mathrm{Cl}^-, \quad k = gl, ax.$$

During action potentials, the ion fluxes through active Na/K pump are

$$J_{p,k}^{Na,dy} = \frac{3\left(I_k^{re} + \Delta I_k\right)}{e}, \quad J_{p,k}^{K,dy} = -\frac{2\left(I_k^{re} + \Delta I_k\right)}{e}, \quad k = gl, ax,$$

where ΔI_k is the variation of current through Na/K pump in the membrane due to the ion concentration changes. The ion fluxes through ion channels can be written as

$$J_{c,k}^{i,dy} = \frac{g_k^{i,dy}}{z^i e}\left(V_k^{re} - E_k^{i,re}\right) + \frac{g_k^{i,dy}}{z^i e}\left(\Delta V_k - \Delta E_k^i\right), \quad k = gl, ax,$$

where $\Delta X_k = X_k^{dy} - X_k^{re}$ is the deviation of X away from the resting state value with $X = V, E, I$ on the membrane *k*. For the conductance on membranes, we have

$$g_{ax}^{Na,dy} = \bar{g}^{Na}(m^{dy})^3 h^{dy} + g_{leak}^{Na}, \quad g_{ax}^{K,dy} = \bar{g}^K (n^{dy})^4 + g_{leak}^K,$$
$$g_{ax}^{Cl,dy} = g_{ax}^{Cl,re}, \quad g_{gl}^{i,dy} = g_{gl}^{i,re}, \quad i = \mathrm{Na}^+, \mathrm{K}^+, \mathrm{Cl}^-,$$

where m^{dy}, h^{dy}, and n^{dy} are governed by system (17). During a single action potential, we claim that the variation of ion's Nernst potential is much smaller than changes in the axon membrane potential (see Appendix A),

$$\Delta E_{ax}^i = o\left(\Delta V_{ax}^*\right), \quad i = \mathrm{Na}^+, \mathrm{K}^+, \mathrm{Cl}^-,$$

At the same time, we estimate that

$$J_{p,ax}^{i,dy} = o\left(\frac{g_{ax}^{i,dy}}{z^i e}\left(V_{ax}^{re} - E_{ax}^{i,re}\right)\right), \quad i = \mathrm{Na}^+, \mathrm{K}^+.$$

This is because the voltage-gated Na^+ and K^+ channels are open during the action potential and satisfy

$$g_{ax}^{i,re} = o\left(g_{ax}^{i,dy}\right), \quad i = \mathrm{Na}^+, \mathrm{K}^+.$$

In addition, the increments of Na/K pump strength are limited since the ion fluxes through the Na/K pump are controlled by its maximum currents $I_{ax,1}$ and $I_{ax,2}$ in Eq. (18).

In sum, during action potentials, we can approximate the axon transmembrane current for each ionic species as

$$I_{ax}^{i,dy} \approx g_{ax}^{i,dy}\left(V_{ax}^{re} - E_{ax}^{i,re}\right) + g_{ax}^{i,dy}\Delta V_{ax}, \quad i = \mathrm{Na}^+, \mathrm{K}^+, \mathrm{Cl}^-. \tag{34}$$

In the next paragraphs, by using Eq. (34), we estimate the accumulative Na^+ and K^+ fluxes through the axon membrane during a single action potential. This estimation helps us estimate the concentration changes in the stimulated extracellular region.

The governing equation of the open probability for Na^+ channel m-gates in the Hodgkin–Huxley model is

$$\frac{dm^{dy}}{dt} = \alpha_m(1 - m^{dy}) - \beta_m m^{dy}, \tag{35}$$

where

$$\alpha_m = \frac{1}{10}\frac{25 - \Delta V_{ax}}{\exp\left(\frac{25 - \Delta V_{ax}}{10}\right) - 1}, \quad \beta_m = 4\exp\left(-\frac{\Delta V_{ax}}{18}\right), \tag{36}$$

and $\Delta V_{ax} = V_{ax}^{dy} - V_{ax}^{re}$. The solution for Eq. (35) is

$$m^{dy}(t) = m_0 \exp\left(\int_0^t \alpha_m(s) + \beta_m ds\right) + \int_0^t \alpha_m(s)\exp\left(-\int_s^t \alpha_m(u) + \beta_m(u)du\right)ds, \tag{37}$$

with initial value m_0.

During a single action potential period $[0, T_{ax}^*]$, we define two distinguished time intervals based on the rapidly responding m-gates open probability m^{dy} as shown in Fig. 6. The first period $[0, t_{m1}]$ is when the Na^+ channel becomes fully open, and the action membrane potential moves positive from its resting value to its most positive value. The second period $[t_{m1}, T_{ax}^* = t_{m1} + t_{m2}]$ occurs when the Na^+ channel closes and the action potential recovers from the peak value to the hyperpolarization value.

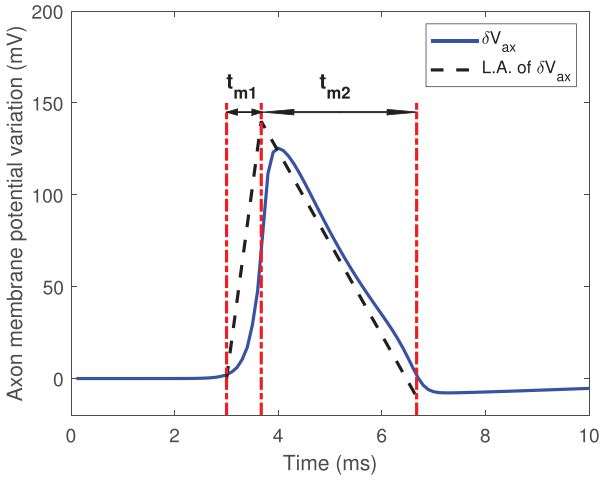

FIG. 6. Two distinguished time intervals used in the estimation during a single action potential. The blue line is the axon membrane potential variation $\Delta V_{ax}(= V_{ax}^{dy} - V_{ax}^{re})$ during a single action potential. The dark dash line is the linear approximation of the ΔV_{ax}. t_{m1} and t_{m2} are the time parameters in Eqs. (B1) and (B2).

In the first time interval $[0, t_{m1}]$, we estimate that ΔV_{ax} increases monotonically from 0 to $E_{ax}^{Na,re} - V_{ax}^{re}$, where we approximate the peak value of action potential by the Nernst potential of Na^+ in the resting state such that

$$\Delta V_{ax}(t) = \frac{E_{ax}^{Na,re} - V_{ax}^{re}}{t_{m1}}t, \quad t \in [0, t_{m1}]. \tag{38}$$

where $E_{ax}^{Na,re} - V_{ax}^{re} \approx 1.4 \times 10^2$ mV. In Eq. (38), the t_{m1} is an unknown variable. The initial value of Eq. (37) is chosen when $\Delta V_{ax} = 0$ mV as

$$m_0 = m^{re} = m^{eq}(0),$$

where m^{eq} is the equilibrium state of Eq. (35) depending on ΔV_{ax},

$$m^{eq}(\Delta V_{ax}) = \frac{\alpha_m(\Delta V_{ax})}{\alpha_m(\Delta V_{ax}) + \beta_m(\Delta V_{ax})}. \tag{39}$$

By using Eqs. (36)–(38), we can obtain one equation for t_{m1} as shown in Eq. (B1) (see Appendix B). Without loss of generality, we assume the voltage-gated Na^+ channel is almost fully open when $t = t_{m1}$ and $m^{dy}(t_{m1}) = 0.95$. The estimation from Eq. (B1) gives $t_{m1} \approx 0.67$ ms.

In the second time interval, we use the homogeneous property of Eq. (35) and move the time interval $[t_{m1}, T_{ax}^* = t_{m1} + t_{m2}]$ to $[0, t_{m2}]$ to simplify the notation. We assume that ΔV_{ax} decreases monotonically from $E_{ax}^{Na,re} - V_{ax}^{re}$ to $E_{ax}^{K,re} - V_{ax}^{re}$ at second time period such that

$$\Delta V_{ax}(t) = E_{ax}^{Na,re} - V_{ax}^{re} - \frac{E_{ax}^{Na,re} - E_{ax}^{K,re}}{t_{m2}}t, \quad t \in [0, t_{m2}], \tag{40}$$

where $E_{ax}^{Na,re} - E_{ax}^{K,re} \approx 1.5 \times 10^2$ mV. We assume that the initial value m_0 of Eq. (37) at the second time period is

$$m_0 = m^{dy}(t_{m1}).$$

The Na^+ channel is in a nearly closed state when the ΔV_{ax} approaching $E_{ax}^{K,re} - V_{ax}^{re}$ and we estimate $m^{dy}(t_{m2}) = 0.1$. In a similar way, by using Eqs. (36), (37), and (40), we could have another equation for t_{m2} as shown in Eq. (B2) (see Appendix B). Based on Eq. (B2), we get $t_{m2} \approx 3$ ms.

In sum, based on estimated t_{m1} and t_{m2} in above, we obtain the approximations for the ΔV_{ax} and the h during a single action potential period ($t \in [0, T_{ax}^* = t_{m1} + t_{m2}]$) as

$$\Delta V_{ax} = \begin{cases} \dfrac{E_{ax}^{Na,re} - V_{ax}^{re}}{t_{m1}}t, & t \in [0, t_{m1}], \\ E_{ax}^{Na,re} - V_{ax}^{re} - \dfrac{E_{ax}^{Na,re} - E_{ax}^{K,re}}{t_{m2}}(t - t_{m1}), & t \in [t_{m1}, T_{ax}^*]. \end{cases}$$

and

$$h^{dy}(t) = h_0 \exp\left(-\int_0^t \alpha_h(s) + \beta_h(s)ds\right) + \int_0^t \alpha_h(s)\exp\left(-\int_s^t \alpha_h(u) + \beta_h(u)du\right)ds,$$

where

$$\alpha_h = \frac{7}{100}\exp\left(-\frac{\Delta V_{ax}}{20}\right), \quad \beta_h = \frac{1}{\exp\left(\frac{30-\Delta V_{ax}}{10}\right)+1},$$

with the initial value h_0

$$h_0 = h^{re}(0) = \frac{\alpha_h(0)}{\alpha_h(0)+\beta_h(0)}.$$

By using Eq. (34), we estimate the cumulative Na^+ flux equations through the axon membrane during a single action potential $[0, T^*_{ax}]$ by

$$\begin{aligned}\int_0^{T^*_{ax}} J^{m,Na,dy}_{ax}\,dt &\approx \int_0^{T^*_{ax}} \frac{\bar{g}^{Na}h^{dy}(m^{dy})^3}{z^{Na}e}\left(V^{re}_{ax}-E^{Na,re}_{ax}\right)+\frac{\bar{g}^{Na}h^{dy}(m^{dy})^3}{z^{Na}e}\Delta V_{ax}\,dt\\ &\approx -2\times10^{-9}\ \mathrm{mol/m^2}. \end{aligned} \tag{41}$$

In the next step, we estimate the cumulative Cl^- flux through the axon membrane during a single action potential $[0, T^*_{ax}]$ by

$$\int_0^{T^*_{ax}} J^{m,Cl,dy}_{ax}\,dt \approx \int_0^{T^*_{ax}} \frac{g^{Cl}_{ax}\Delta V_{ax}}{z^{Cl}e}\,dt \approx -3.7\times10^{-10}\ \mathrm{mol/m^2}. \tag{42}$$

In Eq. (42), we use

$$I^{Cl,dy}_{ax} = g^{Cl}_{ax}\left(V^{re}_{ax}-E^{Cl,re}_{ax}\right)+g^{Cl}_{ax}\left(\Delta V_{ax}-\Delta E^{Cl}_{ax}\right) \approx g^{Cl}_{ax}\Delta V_{ax},$$

since both $V^{re}_{ax}-E^{Cl,re}_{ax}$ and $\Delta E^{Cl}_{ax} = o(\Delta V_{ax})$. In the next, we provide the estimation of the cumulative K^+ flux through axon membrane during a single action potential. The governing equation of ϕ_{ax} yields

$$\sum_i z^i e\frac{\partial}{\partial z}\left(\eta_{ax}j^i_{ax}\right) = -\mathscr{M}_{ax}\left(I^{Na,dy}_{ax}+I^{K,dy}_{ax}+I^{Cl,dy}_{ax}\right). \tag{43}$$

At every location of the stimulated region, the duration of a single action potential is T^*_{ax}. We introduce T^*_{all} for the electrical signal propagation time, during which the signal propagates from one end of the axon (near the optic nerve head) to the other end (far-eye-side of the optic nerve) as shown in Fig. 3. By integrating the right-hand side of Eq. (43) over space $[0, L]$ and time $[0, T^*_{all}]$, we have

$$\begin{aligned}&-\mathscr{M}_{ax}\int_0^{T^*_{all}}\int_0^{L} I^{Na,dy}_{ax}+I^{K,dy}_{ax}+I^{Cl,dy}_{ax}\,dz\,dt\\ &\quad\approx -\mathscr{M}_{ax}L\int_0^{T^*_{ax}} I^{Na,dy}_{ax}+I^{K,dy}_{ax}+I^{Cl,dy}_{ax}\,dt. \end{aligned} \tag{44}$$

where we use the propagation property of the action potential along the z-direction, and only the axon firing period is taken into consideration. By integrating the left-hand side of Eq. (43), we have

$$\int_0^{T^*_{all}}\int_0^{L}\sum_i z^i e\frac{\partial}{\partial z}\left(\eta_{ax}j^i_{ax}\right)dz\,dt = O\left(T^*_{all}e\eta_{ax}j^{bd}_{ax}\right). \tag{45}$$

We assume that the characteristic timescale of T^*_{all} equals $O(10^{-3})$. The scale of ion flux j^{bd}_{ax} at left and right boundaries $(z = 0, L)$ is dominated by the diffusion term

$$j^{bd}_{ax} = O\left(D^*_{ax}\frac{\Delta c^*_{ax}}{z^*}\right),$$

since the boundary conditions are $\frac{\partial\phi_{ax}}{\partial z}|_{z=0,L} = 0$ and $u_{ax}(0) = u_{ax}(L) = 0$. The Δc^*_{ax} is the characteristic difference between ion concentration at boundary value and the ion concentration inside the axon after a single action potential. Based on the Na^+ flux estimation in Eq. (41), we estimate $\Delta c^*_{ax} = O(10^{-1})$. From Eqs. (41) and (42), we get the following order of cumulative fluxes through axon membrane during a single action potential time interval:

$$\begin{aligned}O\left(T^*_{all}\eta_{ax}j^{bd*}_{ax}\right) &\ll O\left(\mathscr{M}_{ax}L\left|\int_0^{T^*_{ax}} J^{m,Cl,dy}_{ax}\,dt\right|\right)\\ &\ll O\left(\mathscr{M}_{ax}L\left|\int_0^{T^*_{ax}} J^{m,Na,dy}_{ax}\,dt\right|\right). \end{aligned} \tag{46}$$

In other words, based on Eqs. (44)–(46), it yields

$$O\left(\left|\int_0^{T^*_{ax}} J^{m,K,dy}_{ax}\,dt\right|\right) = O\left(\left|\int_0^{T^*_{ax}} J^{m,Na,dy}_{ax}\,dt\right|\right). \tag{47}$$

Based on Eq. (41), the cumulative axon transmembrane K^+ flux during a single action potential should be

$$\int_0^{T^*_{ax}} J^{m,K,dy}_{ax}\,dt \approx 2\times10^{-9}\ \mathrm{mol/m^2}. \tag{48}$$

where $[0, T^*_{ax}]$ is the time interval enclosing a single action potential.

Remark 5. Equation (47) shows that for a single action potential, the leading order of the cumulative K^+ flux out of the axon to the extracellular space equals the leading order of the cumulative Na^+ flux into the axon from the extracellular space. This estimation is consistent with observations in the literature.[64–66]

Next, we estimate the concentration variation in the stimulated extracellular region due to a single action potential. The timescale t^* of a single action potential is in milliseconds and during action potential the scale of g^*_{ax} is $\bar{g}^{Na}$. In Appendix A, the scale of axon membrane potential ΔV^*_{ax} is

$$\frac{k_B T}{\Delta V^*_{ax}e} = o(1).$$

Therefore, in Eq. (26) by taking $\delta^i_{10} = \frac{t^*\mathscr{M}_{ax}\bar{g}^{Na}\Delta V^*_{ax}}{c^{i*}_{ax}e}$, we have

$$\left\{\frac{\delta^i_{13}\delta^i_8}{\delta^i_{12}\delta^i_{10}}, \frac{\delta^i_{14}}{\delta^i_{12}\delta^i_{10}}\right\} \subset o(1).$$

Hence, the cumulative ion fluxes through axon transmembrane are the main source changes the ion concentration in the stimulated extracellular region,

$$\eta_{ex}\Delta c^i_{ex} = \mathscr{M}_{ax}\int_0^{T^*_{ax}} J^{m,i,dy}_{ax}\,dt, \quad i = Na^+, K^+, \tag{49}$$

where Δc^i_{ex} is the ith ion's concentration variation from its resting state and η_{ex} is unchanged by Eqs. (5a) and (5b) under timescale $t^* = 10^{-3}$ s. Based on Eqs. (47) and (49), the absolute variation of Na^+ and K^+ concentrations in the stimulated extracellular region due to action potentials, can be written as

$$\Delta c_{sti} = O\left(\frac{\mathscr{M}_{ax}}{\eta_{ex}}\left|\int_0^{T^*_{ax}} J^{m,i,dy}_{ax}dt\right|\right), \quad i = \mathrm{Na}^+, \mathrm{K}^+. \tag{50}$$

In the following discussion, we use Δc_{sti} describes the concentration changes in the stimulated extracellular space after a single action potential,

$$\Delta c_{sti} = 0.12\,\mathrm{mM}. \tag{51}$$

B. Estimation of glial transmembrane potassium flux

In this section, we estimate the glial transmembrane current when the K^+ and the Na^+ concentration vary by Δc_{sti} in the stimulated extracellular region. We also find that the electric field ϕ_{gl} responds immediately to the glial K^+ Nernst potential changes. In the stimulated region, the variation of extracellular electric potential $\Delta\phi_{ex}$ is small in comparison to the variation of glial electric potential $\Delta\phi_{gl}$.

The dominant current through the glial membrane in the stimulated region is through the passive K^+ channel, rather than the Na^+ channel or the Na/K pump. At the same time, in the nonstimulated extracellular region, almost the same amount of K^+ moves from the glial compartment to extracellular space. In other words, both the glial cells and extracellular space in the nonstimulated region participate in the spatial buffering process to help potassium clearance.[67,68]

In the stimulated region, the Nernst potential for K^+ across the glial membrane changes because of the additional potassium Δc^K_{ex} in the extracellular space,

$$\Delta E^K_{gl} = \frac{k_B T}{z^K e}\left(\log\left(1+\frac{\Delta c^K_{ex}}{c^{K,re}_{ex}}\right) - \log\left(1+\frac{\Delta c^K_{gl}}{c^{K,re}_{gl}}\right)\right), \tag{52}$$

where $\Delta c^K_l, l = gl, ex$ are the variations of concentrations in the l compartment. The variation of K^+ concentration in the glial compartment Δc^K_{gl} is a result of the Δc^K_{ex} produced by the glial transmembrane K^+ flux. Recall that the volume fraction (η_{gl}) of the glial compartment is much larger than the extracellular space (η_{ex}). At the same time, based on Eq. (50) and K^+ concentration at resting state, we get

$$\Delta c^K_{ex} = o\left(c^{K,re}_{ex}\right), \quad \frac{\Delta c^K_{gl}}{c^{K,re}_{gl}} = o\left(\frac{\Delta c^K_{ex}}{c^{K,re}_{ex}}\right).$$

Therefore, ΔE^K_{gl} in Eq. (52) can be approximated by its Taylor expansion,

$$\Delta E^K_{gl} \approx \frac{k_B T}{z^K e}\frac{\Delta c^K_{ex}}{c^{K,re}_{ex}}. \tag{53}$$

The variation of K^+ Nernst potential in the stimulated region produces the changes of glial membrane potential ΔV_{gl} and glial compartment electric potential $\Delta\phi_{gl}$. We move on now to estimate the variations of electric potentials in the stimulated extracellular and glial regions.

From the governing equation for ϕ_{ex},

$$\sum_i z^i e\nabla\cdot\left(\eta_{ex}\mathbf{j}^i_{ex}\right) = \sum_i z^i e\mathscr{M}_{gl}\left(J^i_{p,gl}+J^i_{c,gl}\right) + \sum_i z^i e\mathscr{M}_{ax}\left(J^i_{p,ax}+J^i_{c,ax}\right), \tag{54}$$

where

$$\mathbf{j}^i_{ex} = c^i_{ex}\mathbf{u}_{ex} - D^i_{ex}\tau_{ex}\left(\nabla c^i_{ex} + \frac{z^i e}{k_B T}c^i_{ex}\nabla\phi_{ex}\right).$$

We claim that after the axon stops firing, the major current is through glial membrane K^+ channels (see Appendix C). Therefore, the right-hand side of Eq. (54) can be approximated as

$$\sum_i z^i e\mathscr{M}_{gl}\left(J^i_{p,gl}+J^i_{c,gl}\right) + \sum_i z^i e\mathscr{M}_{ax}\left(J^i_{p,ax}+J^i_{c,ax}\right) \approx \mathscr{M}_{gl}g^K_{gl}\left(\Delta V_{gl} - \Delta E^K_{gl}\right). \tag{55}$$

Next, we integrate Eq. (54) over the stimulated region $V_S = \{(r,z,\theta)|r\in[0,r_{sti}], z\in[0,L], \theta\in[0,2\pi]\}$, through which the action potential propagates as shown in Fig. 5. By Eq. (55), we have the approximation of the total current

$$\int_{V_S}\mathscr{M}_{gl}g^K_{gl}\left(\Delta V_{gl} - \Delta E^K_{gl}\right)dv \approx \pi r^2_{sti}L\mathscr{M}_{gl}g^K_{gl}\left(\Delta V_{gl} - \Delta E^K_{gl}\right). \tag{56}$$

In the left-hand side of Eq. (54), by the charge neutrality assumption in Eq. (2), we naturally have

$$\sum_i z^i e c^i_{ex}\mathbf{u}_{ex} = 0.$$

Based on Eqs. (42), (47), and (50), we know that after a single action potential the leading order of ion concentration variations in the stimulated extracellular region are as follows:

$$\Delta c^{Na}_{ex} = -\Delta c_{sti}, \quad \Delta c^K_{ex} = \Delta c_{sti}, \quad \Delta c^{Cl}_{ex} = o(\Delta c_{sti}). \tag{57}$$

Using Eqs. (57) and (33), the diffusion term in the left-hand side of Eq. (54) can be approximated as

$$-\int_{V_S}\sum_i z^i e\nabla\cdot\left(\eta_{ex}D^i_{ex}\tau_{ex}\nabla c^i_{ex}\right)dv \approx 2\pi r_{sti}Le\eta_{ex}D^{\mathrm{diff}}_{ex}\tau_{ex}\frac{\Delta c_{sti}}{r^*}, \tag{58}$$

where $D^{\mathrm{diff}}_{ex} = D^K_{ex} - D^{Na}_{ex}$. In Eq. (58), we claim that the currents through the left $(z=0)$ and right $(z=L)$ boundaries of the stimulated region V_S are much smaller than those through the radial transition region S_T. This is because (1) the ion concentration variations are in the radial direction (between stimulated region and nonstimulated region) and (2) the length scales in the z and r direction are different. Therefore, the radial transition region $S_T = \{(r,z,\theta)|r = r_{sti}, z\in[0,L], \theta\in[0,2\pi]\}$ has a much larger area than the left and right boundaries of V_S.

Similarly, the integration of the electric drift term in the left-hand side of Eq. (54) yields the approximation,

$$-\int_{V_S}\sum_i z^i e\nabla\cdot\left(\eta_{ex}D^i_{ex}\tau_{ex}\frac{z^i e}{k_B T}c^i_{ex}\nabla\phi_{ex}\right)dv \approx 2\pi r_{sti}L\eta_{ex}\sigma_{ex}\frac{\Delta\phi_{ex}}{r^*}, \tag{59}$$

where $\sigma_{ex} = \frac{\tau_{ex}e^2}{k_B T}\sum_i (z^i)^2 D^i_{ex}c^i_{ex}$. From Eqs. (56), (58) and (59), we get

$$\frac{2}{r_{sti}}\left(\frac{\eta_{ex}\tau_{ex}eD_{ex}^{\text{diff}}}{\mathscr{M}_{gl}}\frac{\Delta c_{sti}}{r^*}+\frac{\eta_{ex}\sigma_{ex}}{\mathscr{M}_{gl}}\frac{\Delta\phi_{ex}}{r^*}\right)\approx g_{gl}^K\left(\Delta V_{gl}-\Delta E_{gl}^K\right). \quad (60)$$

At the same time, from the governing equation of ϕ_{gl}

$$\sum_i z^i e\nabla\cdot\left(\eta_{gl}\mathbf{j}_{gl}^i\right)=-\sum_i z^i e\mathscr{M}_{gl}\left(J_{p,gl}^i+J_{c,gl}^i\right), \quad (61)$$

where

$$\mathbf{j}_{gl}^i=c_{gl}^i\mathbf{u}_{gl}-D_{gl}^i\tau_{gl}\left(\nabla c_{gl}^i+\frac{z^i e}{k_BT}c_{gl}^i\nabla\phi_{gl}\right),$$

we obtain the following estimation in a similar way:

$$-\frac{2}{r_{sti}}\frac{\eta_{gl}\sigma_{gl}}{\mathscr{M}_{gl}}\frac{\Delta\phi_{gl}}{r^*}\approx g_{gl}^K\left(\Delta V_{gl}-\Delta E_{gl}^K\right), \quad (62)$$

where $\sigma_{gl}=\frac{\tau_{gl}e^2}{k_BT}\sum_i(z^i)^2D_{gl}^ic_{gl}^i$. We neglect the diffusion and convection terms in Eq. (61) because these terms require much longer time to respond to the extracellular concentration change. Based on Eq. (60) and Eq. (62), we have

$$\Delta\phi_{ex}=-\frac{\eta_{gl}\sigma_{gl}}{\eta_{ex}\sigma_{ex}}\Delta\phi_{gl}-\frac{\tau_{ex}eD_{ex}^{\text{diff}}}{\sigma_{ex}}\Delta c_{sti}. \quad (63)$$

In Appendix D, by matching the orders in both sides of Eq. (62), we claim that $\Delta\phi_{ex}=o(\Delta\phi_{gl})$ in the stimulated region and therefore,

$$\Delta V_{gl}=\Delta\phi_{gl}-\Delta\phi_{ex}=O(\Delta\phi_{gl}). \quad (64)$$

In the next step, we approximate the K^+ current through the leaking K^+ channel on the glial membrane. Based on Eqs. (62) and (64), we get

$$g_{gl}^K\left(\Delta\phi_{gl}-\Delta E_{gl}^K\right)\approx g_{gl}^K\left(\Delta V_{gl}-\Delta E_{gl}^K\right)\approx-\frac{2\eta_{gl}\sigma_{gl}}{r_{sti}\mathscr{M}_{gl}}\frac{\Delta\phi_{gl}}{r^*}. \quad (65)$$

Hence, by Eq. (65), we obtain the relation between ΔE_{gl}^K and $\Delta\phi_{gl}$ as

$$\Delta E_{gl}^K\approx(1+h_\varepsilon)\Delta\phi_{gl}, \quad (66)$$

where

$$h_\varepsilon=\frac{2\eta_{gl}\sigma_{gl}}{r_{sti}\mathscr{M}_{gl}r^*g_{gl}^K}.$$

Based on Eq. (65), it gives us the following approximation:

$$g_{gl}^K\left(\Delta V_{gl}-\Delta E_{gl}^K\right)\approx-\frac{g_{gl}^Kh_\varepsilon}{1+h_\varepsilon}\Delta E_{gl}^K. \quad (67)$$

Furthermore, from Eqs. (63), (66), and (53), we get the approximation

$$\Delta\phi_{ex}\approx-\frac{\eta_{gl}\sigma_{gl}k_BT}{\eta_{ex}\sigma_{ex}(1+h_\varepsilon)z^Ke}\frac{\Delta c_{ex}^K}{c_{ex}^{K,re}}. \quad (68)$$

The variations of electric field $\Delta\phi_{gl}$ in both stimulated and nonstimulated regions are produced without delay by ΔE_{gl}^K in the stimulated region, as described in the governing equation of ϕ_{gl} in Eq. (27). The K^+ leaking current is the major current through the glial membrane in the nonstimulated region as it is in the stimulated region because the current through the ion channel is voltage ϕ_{gl} dependent and K^+ conductance is one dominant ion conductance in the glial membrane

$$g_{gl}^i=o\left(g_{gl}^K\right),\quad i=\text{Na}^+,\text{Cl}^-.$$

In the next steps, we introduce the superscript notation "S" for the stimulated region variables and superscript "NS" for nonstimulated region ones. For the glial transmembrane currents, we have the following approximation:

$$\sum_i z^i e\mathscr{M}_{gl}\left(J_{p,gl}^{S,i}+J_{c,gl}^{S,i}\right)\approx\mathscr{M}_{gl}g_{gl}^K\left(\Delta V_{gl}^S-\Delta E_{gl}^{S,K}\right),$$
$$\sum_i z^i e\mathscr{M}_{gl}\left(J_{p,gl}^{NS,i}+J_{c,gl}^{NS,i}\right)\approx\mathscr{M}_{gl}g_{gl}^K\left(\Delta V_{gl}^{NS}-\Delta E_{gl}^{NS,K}\right).$$

By integration of the ϕ_{gl} Eq. (27) over the stimulated region V_S and the nonstimulated region V_{NS}, respectively, it yields

$$\begin{cases}\int_{V_S}\sum_i z^i e\nabla\cdot\left(\eta_{gl}^S\mathbf{j}_{gl}^{S,i}\right)dv\approx\int_{V_S}\mathscr{M}_{gl}g_{gl}^K\left(\Delta V_{gl}^S-\Delta E_{gl}^{S,K}\right),\\ \int_{V_{NS}}\sum_i z^i e\nabla\cdot\left(\eta_{gl}^{NS}\mathbf{j}_{gl}^{NS,i}\right)dv\approx\int_{V_{NS}}\mathscr{M}_{gl}g_{gl}^K\left(\Delta V_{gl}^{NS}-\Delta E_{gl}^{NS,K}\right).\end{cases} \quad (69)$$

Most of the current between region V_S and region V_{NS} goes through the radial transition region S_T. By Eq. (69) and boundary conditions for ϕ_{gl} we obtain

$$\int_{V_S}\mathscr{M}_{gl}g_{gl}^K\left(\Delta V_{gl}^S-\Delta E_{gl}^{S,K}\right)dv\approx-\int_{V_{NS}}\mathscr{M}_{gl}g_{gl}^K\left(\Delta V_{gl}^{NS}-\Delta E_{gl}^{NS,K}\right)dv. \quad (70)$$

Based on Eq. (70), the average K^+ flux through the glial membrane in the nonstimulated region leaks out to extracellular space with an approximate strength

$$\frac{g_{gl}^K}{z^Ke}\left(\Delta V_{gl}^{NS}-\Delta E_{gl}^{NS,K}\right)=-\frac{r_{sti}^2}{r^{*2}-r_{sti}^2}\frac{g_{gl}^K}{z^Ke}\left(\Delta V_{gl}^S-\Delta E_{gl}^{S,K}\right). \quad (71)$$

In summary, Eqs. (70) and (71) show how the glial compartment in the nonstimulated region serves as spatial buffers and helps clear potassium from the extracellular space outside the stimulated axons.[69]

Remark 6. The glial compartment serves as an important and quick potassium transport device to remove accumulated potassium during the axon firing as shown in Fig. 7.

In the stimulated region, the change in the potassium Nernst potential change makes the glial membrane potential more positive and moves potassium through ion channels into the glial compartment. In the nonstimulated region, since glia is an electrical syncytium, the glial membrane potential simultaneously increases as it does in the stimulated region. However, the glia potassium Nernst potential in the nonstimulated region is not very different from that in the resting state. These potentials produce an outward potassium flux from the glial compartment in the nonstimulated region.

Interacting regions of this sort depend on spatial variables and the properties of the glia as a syncytium. It is difficult to capture these effects in models that do not include space as an independent variable. Even if such compartment models capture these effects correctly in

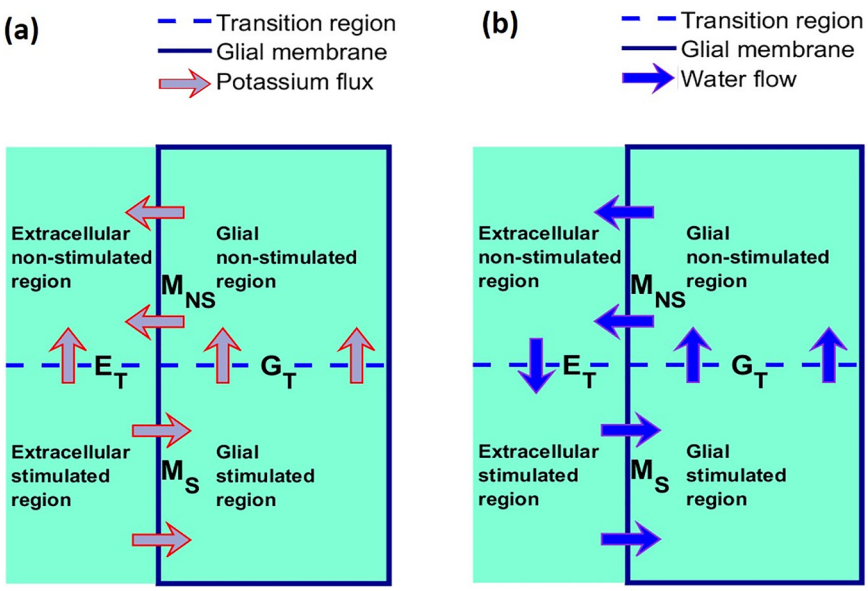

FIG. 7. (a) Schematic graph of the potassium flux when inner part axon stimulated. In the stimulated region, the potassium takes the way of extracellular pathway and through the glial compartment via glial membrane. In the non-stimulated region, the potassium leaks out to the extracellular space through the glial membrane. (b) Schematic graph of the water circulation when inner part axon stimulated. In the stimulated region, the glial transmembrane water flow goes from extracellular space into glial compartment as the effect of osmosis difference. In the extracellular space, water goes from nonstimulated region to stimulated region in radial direction. In the glia compartment goes in the opposite direction. This compartment drawing is given only to aid qualitative understanding.

one set of conditions (because parameters are chosen to make the description correct), they are unlikely to describe the effects of changes in conditions consistently, including membrane potential.

C The water flow: Circulation and estimation

In this section, we discuss water circulation between the stimulated and the nonstimulated regions. As extra K^+ is gradually cleared, it produces an osmotic pressure difference between the intra- and inter- domain, i.e., between the inside the glial compartment and the extracellular space. This osmotic pressure variation drives transmembrane water flow and water circulation in the optic nerve.

Now we consider a train of stimulus stimulated with the frequency f_m in the axon region $(r < r_{sti}, z = z_0)$ during time $[0, T_{sti}]$. The estimation depends on the K^+ and Na^+ concentration variations in the extracellular space and charge neutrality condition. The clearance of extra amount of K^+ (Δc_{ex}^K) in the stimulated extracellular space mostly goes through glial membrane and extracellular pathway (see Appendix E),

$$\frac{d\left(\eta_{ex}\Delta c_{ex}^K\right)}{dt} = -\left(\lambda_{gl}^{m,K} + \lambda_{ex}^K\right)\Delta c_{ex}^K, \tag{72}$$

where

$$\lambda_{gl}^{m,K} = \frac{\mathscr{M}_{gl} g_{gl}^K h_\varepsilon k_B T}{z^K(1+h_\varepsilon)e^2 c_{ex}^{K,re}}, \qquad \lambda_{ex}^K = \frac{2\eta_{ex} D_{ex}^K \tau_{ex}}{r_{sti} r^*}.$$

The $\lambda_{gl}^{m,K}$ presents the effect of glial transmembrane K^+ flux and the λ_{ex}^K describes the spatial effect of the extracellular K^+ transport between the stimulated region and nonstimulated region. This spatial communication is not negligible since λ_{ex}^K is comparable magnitude to the $\lambda_{gl}^{m,K}$. The initial value of Eq. (72) starts with the first stimulus on axon as

$$\Delta c_{ex}^K(0) = \Delta c_{sti},$$

and at the beginning of each period T, there is an additional Δc_{sti} amount of K^+ accumulated in the extracellular space due to the axon firing

$$\Delta c_{ex}^K(iT) = \Delta c_{ex}^K(iT) + \Delta c_{sti}, \ \ i = 1 \ldots n-1,$$

where $n\left(=\frac{T_{sti}}{f_m}\right)$ is the total number of periods. In the above, we view the extracellular K^+ concentration changes due to axon firing as a source term Δc_{sti}.

Remark 7. The concentration in the stimulated extracellular region changes rapidly because of the transmembrane action potentials, as well as the extracellular electric potential ϕ_{ex}. The effect of fluid circulation is the cumulative result of the above ΔO_{ex}. The fluid flows from the nonstimulated region to the stimulated region are dominated by the trans-glia-membrane flow. So, the convection in the extracellular reduces (i.e., flattens) the variation of osmotic pressure.

Remark 8. These effects make our spatially inhomogeneous model quite different from existing ODE models,[64,70] since those ODE models either take the extracellular ion concentration as constant or they do not consider the ion exchange between the extracellular space and other compartments at all. In a recent work, Marte *et al.*[71] introduce a compartment model similar to Eq. (72) by considering ion flux between neuron, glia, and extracellular regions in both the dendrite and soma region. It is always possible to take a field theory and approximate its x dependence into compartments. However, it is quite difficult to know how to describe the parameter dependence, and compartment inter-dependence in such models consistently, and it is probably impossible to describe the parameter dependence and compartment inter-dependence uniquely. These issues are also considered in the Discussion Section.

Field theories show the interdependence as outputs of the analysis. Because field models are consistent, and their solutions are unique, parameter dependence and compartmental interdependence are unique.

In compartment models, different assumptions are possible and difficult to compare. Analysis with different sets of assumed compartments is likely then to give different results in the hands of different

investigators, creating uproductive controversies, and slowing progress. Field models have many fewer assumptions and are more productive. However, they involve considerably more mathematical analysis[45,46] and numerical difficulties. Field models still contain many known parameters (e.g., most structural parameters, capacitance of membranes, conductivity of extra and intraellular solutions) and a number of not well-known parameters, like the properties and distributions of membrane channels (and their ensemble properties) and active transport systems. Direct experimentation is the best way to determine these parameters and modern optical methods in particular, allow many such measurements on scales much smaller than a cell diameter. However, curve fitting to available data is often all that is possible, as in some cases in this paper, with its unavoidable ambiguities.

The time course of Na^+ variation (Δc_{ex}^{Na}) in the stimulated extracellular space is (see Appendix E)

$$\frac{d\left(\eta_{ex}\Delta c_{ex}^{Na}\right)}{dt} = -\lambda_{ex}^{Na,1}\Delta c_{ex}^{Na} + \lambda_{ex}^{Na,2}\Delta c_{ex}^{K}, \tag{73}$$

with the initial condition

$$\Delta c_{ex}^{Na}(0) = -\Delta c_{sti}.$$

There is Δc_{sti} amount of Na^+ flux into axon compartment from the extracellular space at the beginning of each period

$$\Delta c_{ex}^{Na}(iT) = \Delta c_{ex}^{Na}(iT) - \Delta c_{sti}, \quad i = 1\ldots n-1.$$

In Eq. (73), the $\lambda_{ex}^{Na,1}$ describes the effect of extracellular diffusion and $\lambda_{ex}^{Na,2}$ presents the extracellular electric drift between stimulated and nonstimulated regions. In Eq. (73), we have

$$\lambda_{ex}^{Na,1} = \frac{2\eta_{ex}D_{ex}^{Na}\tau_{ex}}{r_{sti}r^*}, \quad \lambda_{ex}^{Na,2} = \frac{2\eta_{gl}\sigma_{gl}D_{ex}^{Na}\tau_{ex}c_{ex}^{Na,re}}{r_{sti}\sigma_{ex}(1+h_\varepsilon)r^*c_{ex}^{K,re}}.$$

In Appendix E, we present the solution of the coupled linear system of (72) and (73). By the charge neutrality condition Eq. (2), the variation of extracellular osmotic concentration is

$$\Delta O_{ex} = 2\left(\Delta c_{ex}^{K} + \Delta c_{ex}^{Na}\right), \tag{74}$$

where Δc_{ex}^{K} and Δc_{ex}^{Na} are written in Eqs. (E14) and (E15).

Notice that sodium and potassium behave differently in the extracellular space. In the extracellular space, the electric drift K^+ flux has a much smaller magnitude in comparison to diffusive K^+ flux, since the scale ratio R_{ex}^{K} between the electric drift term and diffusion term for K^+ is (see Appendix E)

$$R_{ex}^{K} = \frac{\eta_{gl}\sigma_{gl}}{\eta_{ex}\sigma_{ex}(1+h_\varepsilon)} = o(1). \tag{75}$$

However, for Na^+ in the extracellular space, the magnitude of electric drift flux are comparable to diffusive flux since (see Appendix E)

$$R_{ex}^{Na} = \frac{\eta_{gl}\sigma_{gl}}{\eta_{ex}\sigma_{ex}(1+h_\varepsilon)}\frac{c_{ex}^{Na}}{c_{ex}^{K}} = O(1). \tag{76}$$

In the next discussion, we estimate the scales of the glial transmembrane velocity, glial radial velocity, and extracellular radial velocity. The variation in osmotic pressure in the stimulated region is the driving force for the water flow and circulation. Our estimation is based on the equations governing fluid flow and the spatial variation of osmotic pressure.

From the conservation of mass in glial compartment, we have

$$\frac{\partial\eta_{gl}}{\partial t} + \mathscr{M}_{gl}U_{gl}^{m} + \nabla\cdot\left(\eta_{gl}\mathbf{u}_{gl}\right) = 0. \tag{77}$$

Based on Eq. (74), at $t = T_{sti}$, we know there is cumulative osmosis variation $\Delta O_{ex}(T_{sti})$ in the stimulated extracellular region. Since the glial compartment volume fraction (η_{gl}) is larger than the extracellular volume fraction (η_{ex}), we have

$$|\Delta O_{gl}| < |\Delta O_{ex}|.$$

Therefore, we view the ΔO_{ex} is the driving force for hydrostatic pressure variation. At the resting state, Eq. (77) yields

$$\mathscr{M}_{gl}L_{gl}^{m}\left(p_{gl}^{re} - p_{ex}^{re} - \gamma_{gl}k_BT\left(O_{gl}^{re} - O_{ex}^{re}\right)\right) + \nabla\cdot\left(\eta_{gl}^{re}\mathbf{u}_{gl}^{re}\right) = 0,$$

and by Eq. (77), we get

$$\frac{\partial\Delta\eta_{gl}}{\partial t} + \mathscr{M}_{gl}L_{gl}^{m}\left(\Delta p_{gl} - \Delta p_{ex} - \gamma_{gl}k_BT\left(\Delta O_{gl} - \Delta O_{ex}\right)\right) + \nabla\cdot\left(\Delta\left(\eta_{gl}\mathbf{u}_{gl}\right)\right) = 0. \tag{78}$$

Based on Eq. (5a), the scale of the second term in Eq. (78) is much larger than the third term, since

$$\frac{\delta_2}{\delta_1} = \frac{\kappa_{gl}\tau_{gl}}{\mu(r^*)^2\mathscr{M}_{gl}L_{gl}^{m}} = o(1).$$

where we choose

$$U_{gl}^{*} = k_BTO^*, \quad u_{gl}^{*} = \frac{\kappa_{gl}\tau_{gl}k_BTO^*}{\mu r^*}.$$

Therefore, Eq. (78) in the stimulated glial region can be approximated as

$$\frac{\partial\left(\Delta p_{gl} - \Delta p_{ex}\right)}{K_{gl}\partial t} + \mathscr{M}_{gl}L_{gl}^{m}\left(\Delta p_{gl} - \Delta p_{ex}\right) + \mathscr{M}_{gl}L_{gl}^{m}\gamma_{gl}k_BT\Delta O_{ex} = 0, \tag{79}$$

with the initial condition

$$\Delta\eta_{gl}(0) = \frac{\Delta p_{gl}(0) - \Delta p_{ex}(0)}{K_{gl}} = 0.$$

In Eq. (79), we have used the relationship between hydraulic pressures p_l, $l = gl, ex$ and glial compartment volume fraction η_{gl} in Eq. (4a)

$$K_{gl}\Delta\eta_{gl} = \Delta p_{gl} - \Delta p_{ex}. \tag{80}$$

By using a linear approximation of extracellular osmotic concentration variation ΔO_{ex}

$$\Delta O_{ex}(t) = \frac{\Delta O_{ex}(T_{sti})}{T_{sti}}t, \quad t \in [0, T_{sti}],$$

the solution of $\Delta(p_{gl} - p_{ex})$ in Eq. (79) can be written as

$$\Delta p_{gl}(t) - \Delta p_{ex}(t) = \left(\frac{Bt}{A}\exp(At) - \frac{B}{A^2}(\exp(At) - 1)\right)\exp(-At) \tag{81}$$

where

$$A = \mathscr{M}_{gl} L^m_{gl} K_{gl}, \quad B = -K_{gl} \mathscr{M}_{gl} L^m_{gl} \gamma_{gl} k_B T \frac{\Delta O_{ex}(T_{sti})}{T_{sti}}.$$

Hence, we estimate the average glial transmembrane water velocity in the stimulated region as

$$U^m_{gl}(t) = L^m_{gl}\left(\Delta p_{gl}(t) - \Delta p_{ex}(t) + \gamma_{gl} k_B T \Delta O_{ex}(t)\right), \tag{82}$$

and the scale of glial transmembrane velocity in the stimulated region as

$$U^*_{gl} = |U^m_{gl}(T_{sti})|. \tag{83}$$

In Eq. (82), the hydrostatic pressure variations $\Delta p_l, l = gl, ex$ passively react to the osmotic pressure variation $k_B T \cdot \Delta O_{ex}$ in the stimulated region. Therefore, the direction of this glial transmembrane water flow is determined by osmotic pressure variation $k_B T \cdot \Delta O_{ex}$.

In the next step, we estimate the glial radial velocity scale u^{r*}_{gl} and extracellular radial velocity scale u^{r*}_{ex}. By the incompressibility condition, we have

$$\nabla \cdot (\eta_{gl} \mathbf{u}_{gl}) + \nabla \cdot (\eta_{ex} \mathbf{u}_{ex}) + \frac{\partial(\eta_{ax} u^z_{ax})}{\partial z} = 0. \tag{84}$$

In Eq. (84), the dominant terms are the gradients in radial direction, because the length scale difference between r^* and z^* and the osmotic pressure variation are both in the radial direction. Therefore, Eq. (84) can be approximated by

$$\frac{\partial(\eta_{gl} u^r_{gl})}{\partial r} + \frac{\partial(\eta_{ex} u^r_{ex})}{\partial r} = 0, \tag{85}$$

The velocity boundary conditions at $r = 0$,

$$u^r_{gl} = u^r_{ex} = 0,$$

and Eq. (85) yield

$$\eta_{gl} u^r_{gl} + \eta_{ex} u^r_{ex} = 0. \tag{86}$$

With the help of Eq. (86), we can rewrite u^r_{gl} in form of

$$u^r_{gl} = (1 - \chi) u^r_{gl} - \chi \frac{\eta_{ex}}{\eta_{gl}} u^r_{ex}, \tag{87}$$

where the χ is defined as

$$\chi = \frac{\kappa_{gl} \tau_{gl}}{\frac{\eta_{ex}}{\eta_{gl}} \kappa_{ex} \tau_{ex} + \kappa_{gl} \tau_{gl}}.$$

By substituting Eqs. (6) and (10) into Eq. (87), we estimate the radial velocity scale in the glial compartment as

$$u^{r*}_{gl} = \left| (1 - \chi) \frac{\kappa_{gl} \tau_{gl}}{\mu} \frac{\Delta p_{gl} - \Delta p_{ex}}{r^*} - (1 - \chi) \frac{\kappa_{gl} \tau_{gl}}{\mu} \gamma_{gl} k_B T \frac{\Delta O_{gl}}{r^*} - \chi \frac{\eta_{ex}}{\eta_{gl}} k_e \tau_{ex} \frac{\Delta \phi_{ex}}{r^*} \right|_{t = T_{sti}} \tag{88}$$

In Eq. (88), the ΔO_{gl} is due to the changes of the volume fraction of the glial compartment $\Delta \eta_{gl}$ (see Remark 9) can be estimated as

$$\Delta O_{gl} \approx \frac{\eta^{re}_{gl}}{\eta^{re}_{gl} + \Delta \eta_{gl}} O^{re}_{gl} - O^{re}_{gl} = -\frac{\Delta \eta_{gl}}{\eta^{re}_{gl} + \Delta \eta_{gl}} O^{re}_{gl},$$

where $\Delta \eta_{gl}$ can be written by using the Δp_l as in Eq. (80)

$$\Delta \eta_{gl} = \frac{\Delta p_{gl} - \Delta p_{ex}}{K_{gl}}.$$

Furthermore, by Eq. (86), the scale of radial direction extracellular region velocity scale (u^*_{ex}) given by

$$u^*_{ex} = \frac{\eta_{gl}}{\eta_{ex}} u^*_{gl}. \tag{89}$$

Figure 7(b) shows that the water flow exhibits circulation patterns between the extracellular space and glial compartment. The water flow in the glial compartment is from the stimulated region to the nonstimulated region in the radial direction. In extracellular space, the water flow in the radial direction is from the nonstimulated region to stimulated region.

Remark 9. We assume the average total number of molecules (not concentration) in the stimulated glial region does not change since the major glial transmembrane ion flux in the stimulated region is K^+ flux and this K^+ flux from the stimulated extracellular space moves through the glial transition S_t to the nonstimulated extracellular space as Eq. (70).

D. The relative importance of ion flux components

In this section, we discuss the relative importance of ion flux components, due to diffusion, convection, and electric drift in the glial and extracellular regions, respectively. Our discussion focuses on the radial direction since these are the dominant fluxes.

In the extracellular space, we characterize the relative importance of electric drift and diffusion (of potassium and sodium) in the extracellular space by the ratios R^K_{ex} and R^{Na}_{ex} analyzed in Eqs. (75) and (76)

$$R^K_{ex} = \left| \frac{\eta_{gl} \sigma_{gl}}{\eta_{ex} \sigma_{ex}(1 + h_\varepsilon)} \right|, \quad R^{Na}_{ex} = \left| \frac{\eta_{gl} \sigma_{gl}}{\eta_{ex} \sigma_{ex}(1 + h_\varepsilon)} \frac{c^{Na}_{ex}}{c^K_{ex}} \right|.$$

For radial direction flux, the ratio between convection and diffusion in the extracellular space is estimated by the Peclet number shown in Eq. (23)

$$Pe^i_{ex} = \left| \frac{c^i_{ex} u^*_{ex} r^*}{D^i_{ex} \tau_{ex} \Delta c^i_{ex}} \right|, \quad i = \mathrm{Na}^+, \mathrm{K}^+, \tag{90}$$

where we approximate radial diffusion flux scale in the extracellular space as

$$\left| D^*_{ex} \tau_{ex} \frac{\Delta c^i_{ex}}{r^*} \right|, \quad i = \mathrm{Na}^+, \mathrm{K}^+.$$

In a similar way, we estimate the Peclet numbers shown in Eq. (23) in the glial compartment as

$$Pe^i_{gl} = \left| \frac{c^i_{gl} u^*_{gl} r^*}{D^*_{gl} \tau_{gl} \Delta c^i_{gl}} \right|, \quad i = \mathrm{Na}^+, \mathrm{K}^+. \tag{91}$$

Note that the Peclet numbers for Na^+ and K^+ are significantly different due to their different concentrations as shown in Eqs. (90) and

(91). In the glial compartment, the ratio between electric drift and diffusion is

$$R_{gl}^{K} = \left| \frac{1}{1+h_\varepsilon} \frac{c_{gl}^{K} \Delta c_{ex}^{K}}{c_{ex}^{K} \Delta c_{gl}^{K}} \right|, \quad R_{gl}^{Na} = \left| \frac{1}{1+h_\varepsilon} \frac{c_{gl}^{Na} \Delta c_{ex}^{K}}{c_{ex}^{K} \Delta c_{gl}^{Na}} \right|. \tag{92}$$

where we have used Eqs. (53) and (66). In Eq. (92), we estimate the K^+ concentration change (Δc_{gl}^{K}) in the stimulated glial compartment as

$$\Delta c_{gl}^{K} \approx \left(n c_{sti} - \Delta c_{ex}^{K}\right) \frac{\lambda_{gl}^{m,K}}{\lambda_{gl}^{m,K} + \lambda_{ex}^{K}} \frac{\eta_{ex}}{\eta_{gl}}, \tag{93}$$

where $\lambda_{gl}^{m,K}$ and λ_{ex}^{K} are defined in Eq. (72), and n is the number of stimuli.

We estimate the Δc_{gl}^{Na} in the stimulated glial compartment as

$$\Delta c_{gl}^{Na} \approx -\frac{3\Delta I_{gl}}{g_{gl}^{K}\left(\Delta V_{gl} - \Delta E_{gl}^{K}\right)} \Delta c_{gl}^{K}, \tag{94}$$

where ΔI_{gl} are approximated by Taylor expansion as

$$\Delta I_{gl} \approx 2\left(\frac{\mathrm{K}_{\mathrm{K1}} I_{gl}^{re,1}}{c_{ex}^{K,re}\left(c_{ex}^{K,re} + K_{K1}\right)} + \frac{\mathrm{K}_{\mathrm{K2}} I_{gl}^{re,2}}{c_{ex}^{K,re}\left(c_{ex}^{K,re} + K_{K2}\right)} \right) \Delta c_{ex}^{K}.$$

In Sec. V, we carry out a numeric simulation as mentioned previously. Furthermore, we compare the results between the electrodiffusion model with the convection–electrodiffusion (full) model.

V. NUMERICAL SIMULATION

In this section, numerical simulations are used to confirm our asymptotic estimations. The comparison between electrodiffusion model and the full convection–electrodiffusion model is conducted to understand how the nervous (neuron–glia) system interacts with the extracellular space to create microcirculation.

A train of stimuli is applied to stimulate the axon membrane near the left boundary ($\{(z_0, r)|z_0 = 1.875\,\mathrm{mm}\,\mathrm{and}\,r < r_{sti} = \frac{1}{2}r^* = 24\,\mu\mathrm{m}\}$). Each single stimulus has current strength $I_{sti} = 3 \times 10^{-3}\,\mathrm{A/m^2}$ with duration 3 ms. The frequency of the stimuli is 50 Hz ($T = 0.02$ s) and the duration is $T_{sti} = 0.2$ s. The obtained full model is solved by using finite-volume method with mesh size $h = 1/20$ and temporal size $t = 1/10$ in dimensionless. The code is written in the Matlab environment.

A. Estimation of velocity scales

We first estimate how large are the fluid velocities in extracellular space and glial compartment generated by a train of stimuli. From Eqs. (E15) and (E14), the estimated concentration variations in the stimulated extracellular region at $t = T_{sti}$ are

$$\Delta c_{ex}^{Na} \approx -1.06\,\mathrm{mM}, \quad \Delta c_{ex}^{K} \approx 0.89\,\mathrm{mM}, \quad \Delta O_{ex} \approx -0.34\,\mathrm{mM}.$$

The estimated glial transmembrane velocity by Eq. (88) is

$$U_{gl}^{*} \approx 9.78 \times 10^{-2}\,\mathrm{nm/s}.$$

From Eqs. (88) and (89), the estimated scale of radial water velocities inside glial compartment and extracellular space are

$$u_{ex}^{*} \approx 1.56 \times 10^{1}, \quad u_{gl}^{*} \approx 3.90\,\mathrm{nm/s}.$$

In Figs. 8(a)–8(c), we plot the computed average variation of concentrations in the stimulated extracellular region. These computed concentration changes are consistent with the estimates presented previously. The change of concentration reaches its peak at the end of the train of stimulus ($t = T_{sti}$) and quickly returns to its previous equilibrium value.

In Fig. 8(f), we plot the computed average transmembrane water flow through the glial membrane in the stimulated region. We see Fig. 7(b) that water flows into the glial compartment from the extracellular space in the stimulated region. This transmembrane water flow

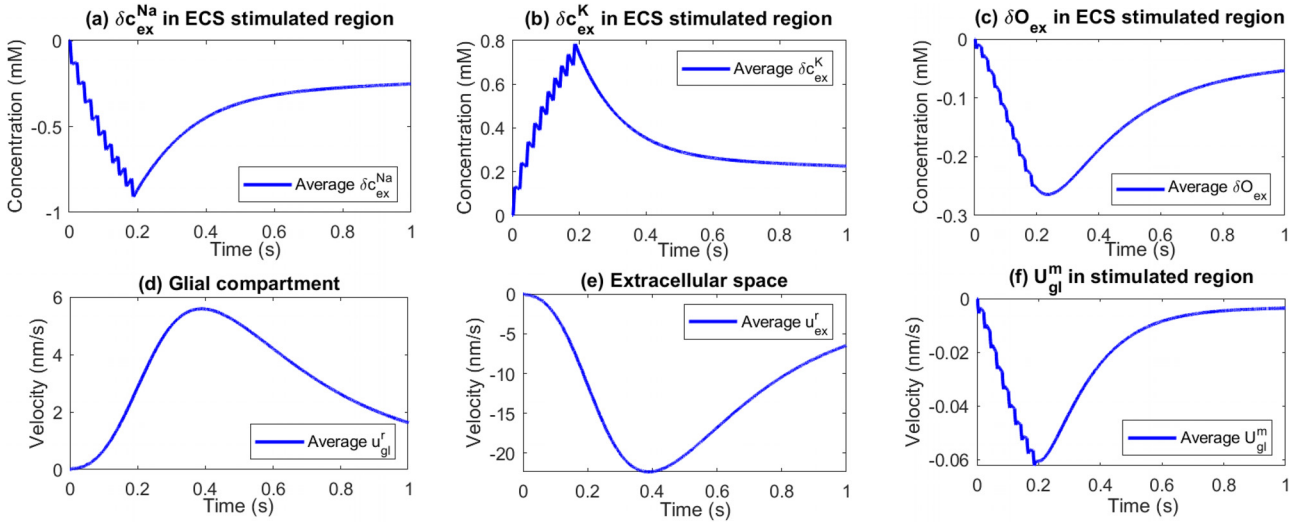

FIG. 8. Numerical results. (a)–(c) Average concentration variations in the stimulated extracellular region; (d) and (e) average radial velocity in the intradomain; (f) average glial transmembrane velocity in the stimulated region (with normal direction points to ECS).

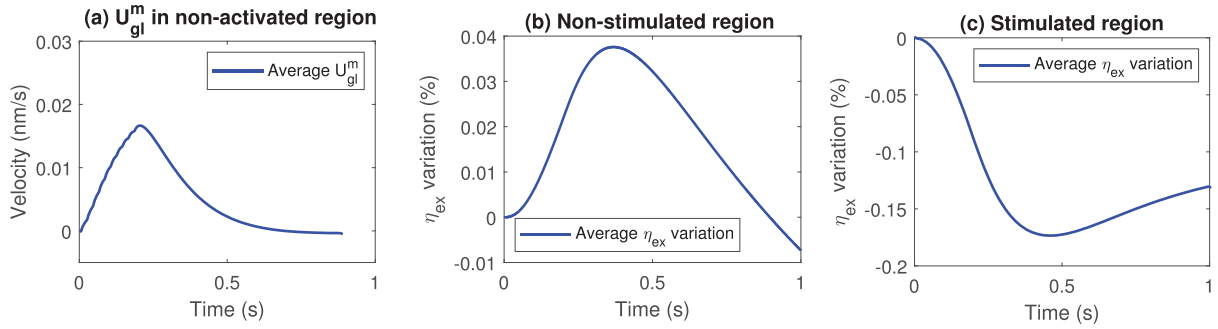

FIG. 9. (a) Average glial transmembrane velocity in the nonstimulated region (the normal direction points from glial compartment to extracellular space). (b) and (c) Average variation of the extracellular volume fraction in nonstimulated region and stimulated regions.

generates the water circulation between the stimulated region and nonstimulated region in the radial direction. As in Fig. 7(b), in the extracellular compartment, the water flow goes from the nonstimulated region to the stimulated region and in the glial compartment, water flows in the opposite (radial) direction. In Figs. 8(d) and 8(e), we plot the computed average water velocity in the radial direction in the glial compartment and in the extracellular space. The computations are consistent with our estimation above.

In Fig. 9(a), we show the transmembrane water flow through the glial membrane in the nonstimulated region as in Fig. 7(b). This water flow to the extracellular space produces widening of the extracellular space volume in the nonstimulated region, as shown in Fig. 9(b). At the same time, the extracellular space volume shrinks (in the stimulated region) as shown in Fig. 9(c). The shrinkage is produced by the inward water flow through the glial membrane in the stimulated region, as in Fig. 9(f). In Figs. 10 and 11, the variations of volume fractions of the extracellular space and glial compartment in the whole domain are plotted at time $t = 0.1\,\mathrm{s}$ (during the stimulus), $t = 0.5\,\mathrm{s}$ (maximum variations) and $t = 2\,\mathrm{s}$ (back to resting state). Our simulation is consistent with the experiments in Refs. 72 and 73, where the extracellular space becomes smaller in the middle cortical layers (where the stimulus is applied) but widens in the most superficial and deep cortical layers (where no stimulus is applied).

Remark 10. In Figs. 10 and 11, it is an illusion that there are jumps in the contours of volume fractions for extracellular space and glial compartment. By checking a line-plot at a fixed radius $r = 1.5\,\mu\mathrm{m}$, Fig. 16 in Appendix F illustrates that there are not jumps rather than local extreme values at the $z_0 = 1.875$ mm where the stimuli are applied. These stimuli result in the local potassium accumulation that decreases the osmosis variation in the extracellular space near z_0 (see Appendix F, Fig. 18). Therefore, less shrunken of the extracellular volume fraction near z_0 as Figs. 10 and 11 shown.

B. Importance of convection

In this section, we explore the importance of fluid convection during potassium clearance in each region. We first examine the estimated Peclet numbers for Na^+ and K^+ in the extracellular and glial compartments. By Eq. (90), the Peclet numbers (for the radial ion flux) in the extracellular space are

$$Pe_{ex}^{K} = \left| \frac{c_{ex}^{K} u_{ex}^{*} r^{*}}{D_{ex}^{K} \tau_{ex} \Delta c_{ex}^{K}} \right| \approx 1.0 \times 10^{-2},$$
$$Pe_{ex}^{Na} = \left| \frac{c_{ex}^{Na} u_{ex}^{*} r^{*}}{D_{ex}^{Na} \tau_{ex} \Delta c_{ex}^{Na}} \right| \approx 3.5 \times 10^{-1}.$$

By Eqs. (75) and (76), the ratios between electric drift and diffusion (of the radial ion flux) in the extracellular space are

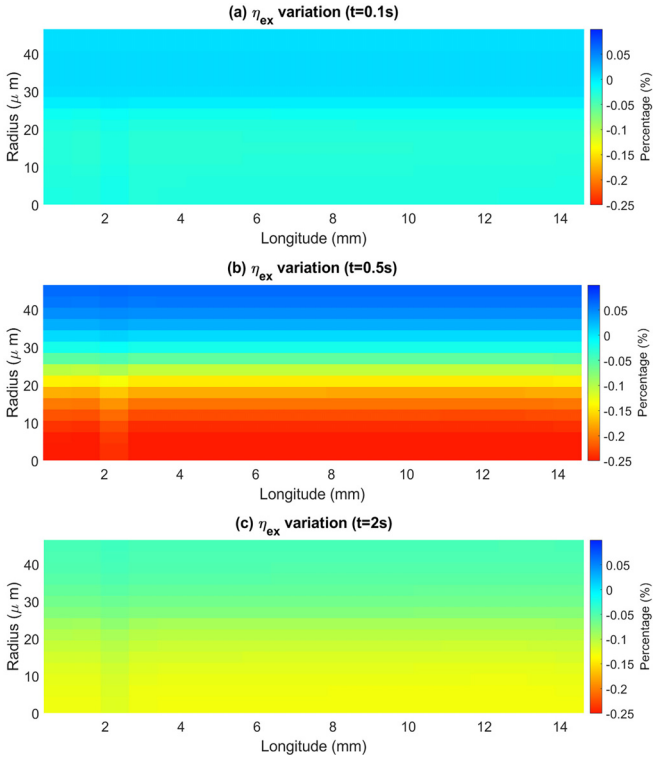

FIG. 10. (a)–(c) Extracellular space volume fraction (η_{ex}) variation at time $t = 0.1$s, 0.5s, 2s. The blue is the enlarged region of extracellular space and red is the shrunken region of the extracellular space which is qualitatively consistent with the results in Refs. 72 and 73. The stimulus current has been applied at $z_0 = 1.875$ mm as shown in Fig. 5, which induces ion concentration and osmosis variation differ. The volume fraction changes depend on the hydrostatic pressure difference which involves the osmotic pressure (see Fig. 18 in Appendix F).

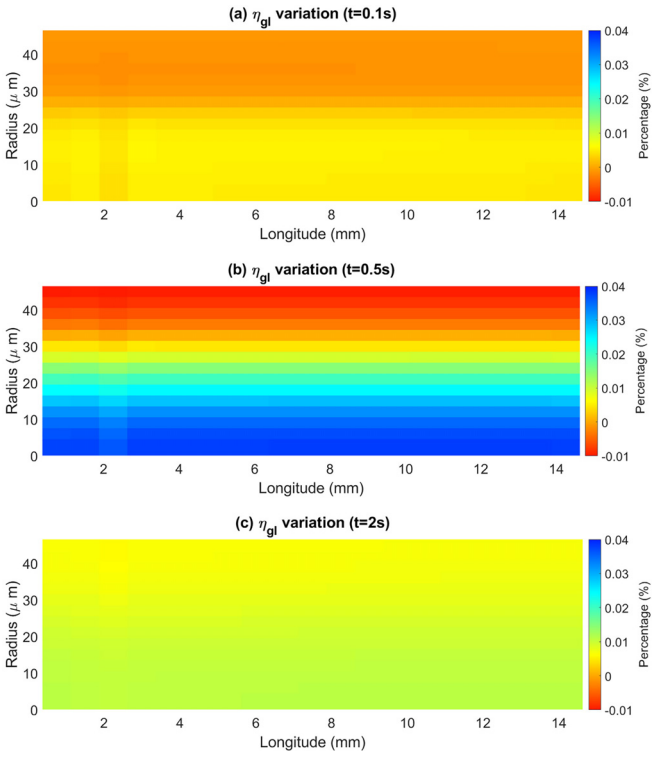

FIG. 11. (a)–(c): Glial compartment volume fraction (η_{gl}) variation at time $t = 0.1$s, 0.5s, 2s.

$$R_{ex}^{K} = \left| \frac{\eta_{gl}\sigma_{gl}}{\eta_{ex}\sigma_{ex}(1+h_\varepsilon)} \right| \approx 6.2 \times 10^{-2},$$

$$R_{ex}^{Na} = \left| \frac{\eta_{gl}\sigma_{gl}}{\eta_{ex}\sigma_{ex}(1+h_\varepsilon)} \frac{c_{ex}^{Na}}{c_{ex}^{K}} \right| \approx 2.3.$$

In the glial compartment, based on Eqs. (91), (93), and (94), we get the Peclet numbers (for the radial ion flux) as

$$Pe_{gl}^{K} = \left| \frac{c_{gl}^{K} u_{gl}^{*} r^{*}}{D_{gl}^{K} \tau_{gl} \Delta c_{gl}^{K}} \right| \approx 2.9 \times 10^{1},$$

$$Pe_{gl}^{Na} = \left| \frac{c_{gl}^{Na} u_{gl}^{*} r^{*}}{D_{gl}^{Na} \tau_{gl} \Delta c_{gl}^{Na}} \right| \approx 1.7 \times 10^{1}.$$

By Eq. (92), the ratios between electric drift and diffusion (of the radial ion flux) in the glial compartment are

$$R_{gl}^{K} = \left| \frac{1}{1+h_\varepsilon} \frac{c_{gl}^{K} \Delta c_{ex}^{K}}{c_{ex}^{K} \Delta c_{gl}^{K}} \right| \approx 4.3 \times 10^{2},$$

$$R_{gl}^{Na} = \left| \frac{1}{1+h_\varepsilon} \frac{c_{gl}^{Na} \Delta c_{ex}^{K}}{c_{ex}^{K} \Delta c_{gl}^{Na}} \right| \approx 1.7 \times 10^{2}.$$

In Fig. 12, we plot the computed potassium and sodium fluxes (in the radial direction) in the extracellular space and glial compartments.

In the extracellular space, the importance of different fluxes is complicated because they depend on the ion species concentration as shown in Eq. (90). For potassium, the diffusion flux is dominant as shown in Fig. 12(a), upper panel. Except for sodium [Fig. 12(a), lower panel], the three fluxes, diffusion, convection, and electric drift, are comparable with the electric drift flux being somewhat larger. These simulation results agree with our estimations above. In the extracellular space, the potassium's Peclet number Pe_{ex}^{K} and the ratio R_{ex}^{K} are in $O(10^{-2})$, while the sodium's Peclet number Pe_{ex}^{Na} is order of $O(10^{-1})$ and the ratio R_{ex}^{Na} is in $O(1)$.

In the glial compartments [Fig. 12(b)], the situation is different from the extracellular space. The electric drift is dominant, and convection flux comes as second in importance for both sodium and potassium. The water flow has a more important effect on potassium

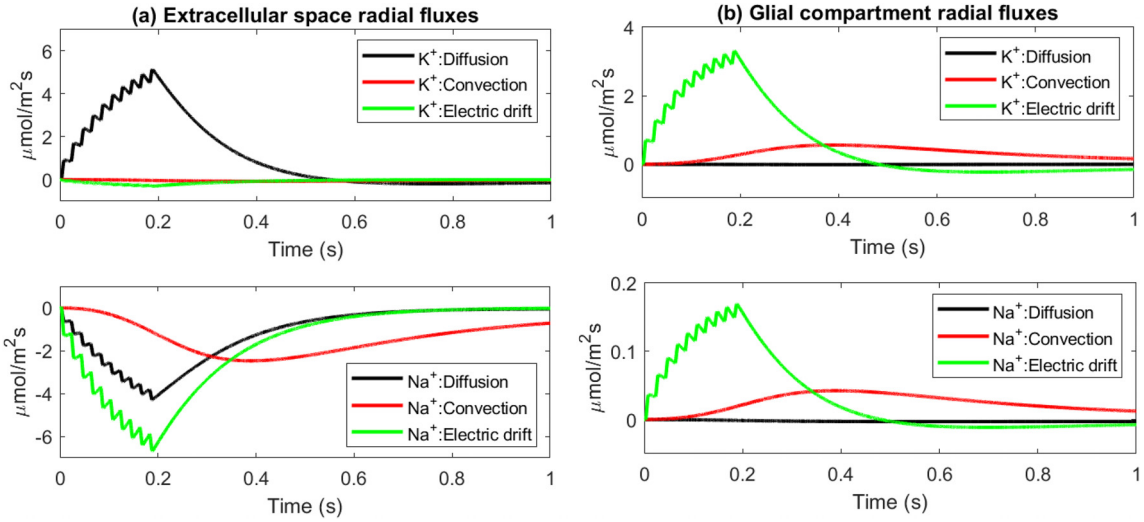

FIG. 12. (a) Average radial direction fluxes components in the extracellular space. (b) Average radial direction fluxes components in the glial compartment (radial direction as normal direction).

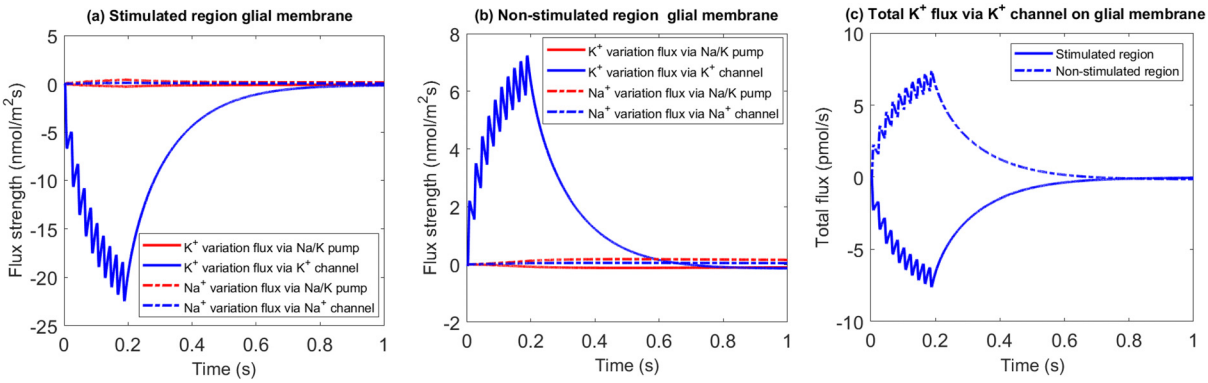

FIG. 13. (a) Potassium and sodium flux variation through Na/K pump and ion channels on the glial membrane in the stimulated region. (b) Potassium and sodium flux variation through Na/K pump and ion channels on the glial membrane in the nonstimulated region. c: the total potassium flux through potassium channel on the glial membrane.

in the glial compartment than in the extracellular space. The maximum of the convection flux occurs after the stimuli, since it takes that long for osmotic pressure to accumulate. Also, it lasts longer time when the effect of electric drift has diminished.

In Figs. 13(a) and 13(b), the potassium and sodium flux through the glial membrane are presented and the results are consistent with our estimates. The major current through the glial membrane is through the potassium channel in both stimulated region and nonstimulated region. Figure 13(c) compares the stimulated and nonstimulated region by showing the total potassium flux through potassium channels (integrated over all the glial membrane). The total potassium flux has different direction in the stimulated region and nonstimulated region, as shown in our estimation in Eq. (70). The strength is the same, but the direction is different.

Figure 14 compares the potassium flux in the electrodiffusion (ED) model and convection–electrodiffusion (full) model. In the full model, the water circulation between the stimulated and nonstimulated region in both extracellular and glial compartments have an important role in the circulation of potassium. The water circulation has an important role in buffering potassium in the optic nerve bundle. The water circulation increases the potassium flow through the glial compartment.

Figure 14(b) show how water flow increases the potassium flux through the glia in the transition region between the stimulated and nonstimulated region. The potassium flux moves back to the stimulated extracellular region from nonstimulated extracellular region through the extracellular pathway, as shown in Fig. 14(a). The time rate of change of the cumulative K^+ flux through the extracellular transition region decreases after stimulus.

Multiple trains of action potentials strengthen the effect of water flow on the transport through the glial compartment. In Fig. 15, three trains of action potentials occur with 0.2 s resting period between each. Figure 15(b) shows that water flow increases 25% of the amount of cumulative potassium flux through the transition region in the glial compartment, beyond the potassium flow in the electrodiffusion model. Consequently, the amount of cumulative potassium flux through the transition region in the extracellular space is around 15% less than in the electrodiffusion model [see Fig. 15(a)].

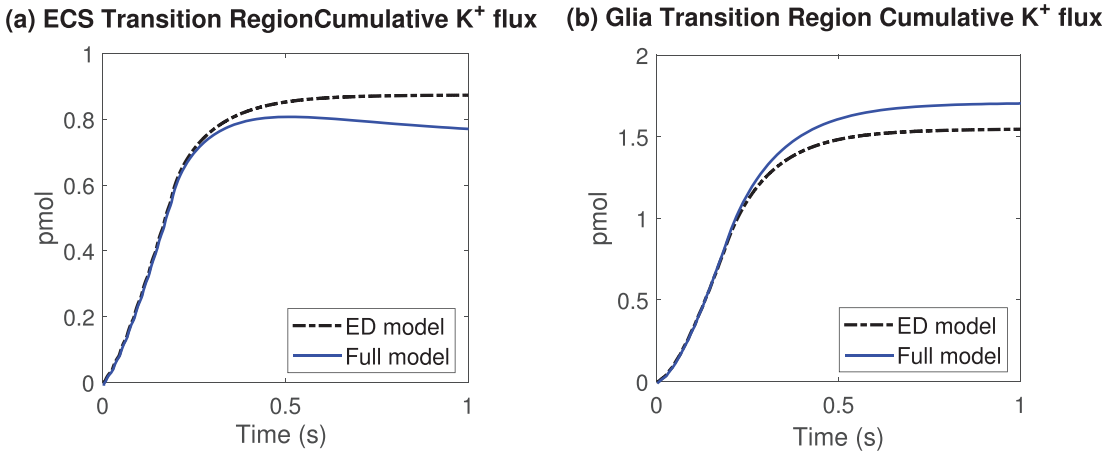

FIG. 14. (a) Cumulative K^+ flux on extracellular transition region. (b) Cumulative K^+ flux on glail transition region (radial direction as normal direction).

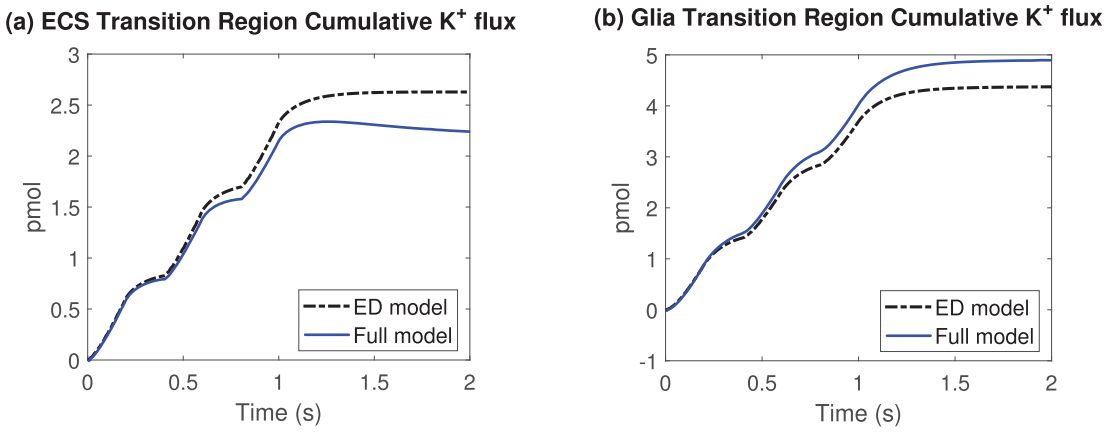

FIG. 15. Multiple trains of action potentials. (a) Cumulative K^+ flux on extracellular transition region. (b) Cumulative K^+ flux on glail transition region (radial direction as normal direction).

VI. DISCUSSION

Biological systems, like engineering systems, are complex, involving many components connected in specific structures, using a range of forces to perform specific functions, often that can be defined by quantitative measurements and relations. These systems are defined in textbooks of physiology and some in more mathematical detail elsewhere.

Many parameters are involved that need to be known if function is to be understood and predicted. What is not so well known is how these parameters are determined. In one extreme, the circuits of electronic devices all parameters—every one—are known by independent measurements. Curve fitting is not involved at all. Indeed, it is hard to imagine how a computer of some 10^{13} devices that interact with each other some 10^9 times a second could function if parameters were not definite and known to the designer of the circuit. Thus, complexity in itself does not prevent definite understanding.

A crucial help in dealing with electronic circuits is the universal and exact nature of the Maxwell equations that govern electronic current flow in these structures. The same equations are true for biological systems for ions, but the mechanical response of the system to the charges and their movement when electric fields change (loosely called "polarization") is not so well known. Measurements of the physical and electrical structure of tissues are, however, sometimes possible giving some of the certainty to fortunate biological systems that the Maxwell–Kirchhoff equations bring to electronic systems. It is natural to try to simplify the electrical and then the electrodiffusional and osmotic properties of biological tissues with compartment models, in which spatial variables and differential equations in space and time are replaced by compartments and ordinary differential equations in time. These compartments can be derived in some cases by well-defined perturbation procedures (some of which we use here) but the accuracy of the perturbation scheme and reduced models is difficult to determine, to put it mildly, given the large number of parameters that affect that accuracy, particularly as conditions change. The compartments introduce a level of uncertainty that is hard to resolve and is likely to impede agreement among investigators and thus the progress of knowledge. In some fortunate cases, biological systems are known well. Then field equations can be written and solved that are general and quite independent of the choice of compartments, as we have tried to do here. The system of long cylindrical nerve fibers, ionic channels, and membranes—particularly their capacitance—that conducts the signals (action potentials) of the nervous system is known quite well. Independent measurements of every component are available. Parameters can be measured of almost all components in several independent ways that give indistinguishable results. Thus action potential propagation can be computed with little ambiguity.

Some syncytial tissues are known almost this well. The lens of the eye has been studied by impedance spectroscopy and morphometry so the structure and structural parameters are well known. Flows have been directly measured and also pressure, sometimes with spatial dependence, in Mathias group more than anywhere else In the case of the lens, the biological system is nearly as well determined as the electronic system. The optic nerve is not so well known. Here we have good structural information but limited knowledge of parameters. Membrane capacitance and extracellular and intracellular resistivities are known. Conductance of voltage-activated channels and connexins is known but the spatial distribution of connexins and channels is not known, and even the identity of the channels is not known. Thus calibration of our optic nerve model is incomplete, as we have tried to explain in detail in the text, and so validation is limited as well. What is needed for calibration in the optic nerve more than anything else is experimental measurements of the type and spatial distribution of pumps and channels. What is needed for validation is experimental measurements of the spatial distribution of potentials, concentrations, and pressures. The theory can easily be extended to compute those quantities not already included. Indeed, this process of calibration and validation is what is needed, in our view, to understand the role of water flow, ion migration, and diffusion in other systems in the central nervous system. Understanding the glymphatic flows in the central nervous system requires a field theory in the spirit of that presented here. It requires calibration with the spatial distribution of pumps and channels. It requires validation by measurement of the spatial distribution of concentration, electrical potential, and pressure. A validated and calibrated theory can then predict and understand the glymphatic flows so important in biological processes like sleep and pathological situations like migraine and epilepsy.

VII. CONCLUSION

This work provides a comprehensive set of estimates and computations, showing the water circulation in the optic nerve. The water flow is generated by the osmotic difference between the glial compartment and extracellular space. Through the estimation, we show that in the stimulated region, the extracellular osmotic changes are not induced by ion fluxes from the axon compartment when the axon is firing. Indeed, based on the analysis, we found that the leading order of potassium flux out and sodium flux into the axon is the same during the action potential, which is consistent with the literature.[64,65] The osmotic difference is generated due to the sodium and potassium conductance difference in the glial membrane. In other words, more potassium leaks into the glial compartment, and less sodium leaks out. As a result of this glial transmembrane water flow in the stimulated region, it forms a water circulation in the radial direction between the stimulated region and the nonstimulated region.

Our estimation of the velocity scales in the glial compartment and extracellular space shows that this water flow has a considerable effect on potassium flux in the glial compartment. By comparing the full model (including water) with the electrodiffusion model (excluding water), we validate that water circulation through the glial pathway helps clear potassium from the extracellular space and enhances the glial buffering effect. With additional numerical simulations, we show that the repetitive activity of the nerve fibers further increases the importance of water flow and the water flow contribution to glia buffering, which is likely to dramatically dominate pathological situations of repetitive activity.

Besides, through our analysis, we show that the electrical syncytium property of the glial cells is critical for clearing potassium (from the extracellular space) when the neuron fires. Based on the governing equation of glial electric potential, we explain why the inward glial transmembrane potassium flux in the stimulated region is almost the same as the outward potassium flux out to the extracellular space in the nonstimulated region when axon firing. This is because the electric potential spreads through the connected cells in the glial compartment. The glial electric potential in the nonstimulated region becomes more positive in response to the depolarization of the glial electric potential in the stimulated region. This electric property for the glial compartment always exists as long as there exist two distinguish stimulated region and nonstimulated region. The glial wraps the axon like a faster potassium transporter, which quickly removes the extra potassium (in the extracellular space) from the stimulated region to the nonstimulated region.

Finally, we would like to point out that the coupling of ionic and water flows is not unique to the optic nerve. It is ubiquitous in many parts of the mammalian body and other biological tissues. Our analysis of the model for the optic nerve is just a first small step toward the understanding of the mechanisms of various transport processes and the consequences of a disrupted process under pathological conditions.

AUTHORS' CONTRIBUTIONS

Y.Z., S.X., and H.H. did the model derivations and carried out the numerical simulations. R.S.E. and H.H. designed the study, coordinated the study, and commented on the manuscript. All authors gave final approval for publication.

ACKNOWLEDGMENTS

This research was supported in part by the National Natural Science Foundation of China under No. 12071190 (S.X.), the Fields Institute for Research in mathematical Science (S.X., R.S.E., and H.H.), and the Natural Sciences and Engineering Research Council of Canada (H.H.). The authors also would like to thank anonymous reviewers for their valuable suggestions on model calibration and validation.

NOMENCLATURE

A_l	Negative charged protein density in l region
c_l^i	Ion i concentration in the l region
g_k^i	Conductance of k membrane for ion i
g_{leak}^i	Leak conductance of axon membrane for ion i
$\bar{g}^i$	Maximum conductance of axon membrane for ion i
$J_{c,k}^i$	Passive transmembrane source of k membrane
$J_{p,k}^i$	Active ATP based ion i pump on k membrane
K_k	Stiffness constant of k membrane
κ_l	Water permeability of l region
L_k^m	Membrane hydrostatic permeability of k membrane
$\mathscr{M}_k$	Membrane area k in per unit control volume
O_l	Osmotic concentration in l region
p_l	Hydrostatic pressure in l region
$\mathbf{u}_l$	Fluid velocity inside of the l region
z^i	Valence of the ion i
η_l	Volume fraction of l region
μ	Fluid viscosity
τ_l	Tortuosity of l region
ϕ_l	Electric potential in l region

APPENDIX A: COMPARISON BETWEEN MEMBRANE POTENTIAL AND NERNST POTENTIAL ON AXON MEMBRANE

The classical Hodgkin–Huxley analysis of a single action potential[74] assumes that changes in concentration of ions are much less important than current flow in determining the shape of the action potential. In other words, the change in the Nernst (i.e., equilibrium) potential is much less than the change in the membrane potential. In this section, we show that the variation of the Nernst potential for Na^+, K^+ and Cl^- on the axon membrane is much smaller than the axon membrane potential changes during action potentials,

$$\Delta E_{ax}^i = o\left(\Delta V_{ax}^*\right), \quad i = \mathrm{Na}^+, \mathrm{K}^+, \mathrm{Cl}^-.$$

During action potentials, the scale of the ΔV_{ax} can be approximated by the Na^+ and K^+ Nernst potential difference at the resting state,

$$\Delta V_{\mathrm{ax}}^* = O\left(E_{ax}^{Na,re} - E_{ax}^{K,re}\right). \tag{A1}$$

We take the Cl^- Nernst potential for example. By the charge neutrality condition in Eq. (2), we have

$$\Delta c_{ax}^{Cl} \approx -\frac{\eta_{ex}}{\eta_{ax}} \Delta c_{ex}^{Cl}. \tag{A2}$$

Therefore, the variation of Cl^- Nernst potential on axon membrane yields

$$\Delta E_{ax}^{Cl} = V^*\left(\log\left(\frac{c_{ex}^{Cl,re}+\Delta c_{ex}^{Cl}}{c_{ax}^{Cl,re}+\Delta c_{ax}^{Cl}}\right)-\log\left(\frac{c_{ex}^{Cl,re}}{c_{ax}^{Cl,re}}\right)\right)$$
$$\approx V^*\left(\log\left(1+\frac{\Delta c_{ex}^{Cl}}{c_{ex}^{Cl,re}}\right)-\log\left(1-\frac{\eta_{ex}\Delta c_{ex}^{Cl}}{\eta_{ax}c_{ax}^{Cl,re}}\right)\right), \quad \text{(A3)}$$

where

$$V^* = \frac{k_B T}{e}, \quad \frac{1}{c_{ex}^{Cl,re}} = O(10^{-2}), \quad \frac{\eta_{ex}}{\eta_{ax}c_{ax}^{Cl,re}} = O(10^{-2}).$$

In addition, the characteristic time for a single action potential T_{ax}^* is in millisecond level $(O(10^{-3}))$, so the scale of Δc_{ex}^{Cl} in the stimulated region is

$$\Delta c_{ex}^{Cl,*} = \Delta c_{ex}^{Na,*} + \Delta c_{ex}^{K,*} < O\left(\frac{T_{ax}^* \mathscr{M}_{ax}\bar{g}^{Na}\Delta V_{ax}^*}{e\eta_{ex}}\right) = O(1), \quad \text{(A4)}$$

where we use charge neutrality condition and maximum conductance of the voltage-gated Na^+ channel. Therefore, Eq. (A3) yields

$$\Delta E_{ax}^{Cl} \approx V^*\left(\frac{1}{c_{ex}^{Cl,re}}+\frac{\eta_{ex}}{\eta_{ax}c_{ax}^{Cl,re}}\right)\Delta c_{ex}^{Cl}, \quad \text{(A5)}$$

Based on Eqs. (A1), (A5), and (A4), and the fact that $\frac{V^*}{\Delta V_{ax}^*} = o(1)$, we have $\Delta E_{ax}^{Cl} = o(\Delta V_{ax}^*)$. In a similar way, we can get

$$\Delta E_{ax}^{i} = o\left(\Delta V_{ax}^*\right), \quad i = Na^+, K^+. \quad \text{(A6)}$$

APPENDIX B: ESTIMATIONS OF t_{m1} AND t_{m2}

In this section, we provide estimations on t_{m1} and t_{m2}. For the first time interval parameter t_{m1}, by substituting Eqs. (36) and (38) into Eq. (37), we obtain

$$m^{dy}(t_{m1}) = m_0 \exp\left(\frac{18t_{m1}}{35}\left(\exp\left(\frac{-70}{9}\right)-1\right)\right.$$
$$+\frac{t_{m1}}{14}\left[\mathrm{Li}_2(\exp(x))+x\ln(1-\exp(x))-\frac{1}{2}x^2\right]\Big|_{2.5}^{-11.5}\Big)$$
$$-\frac{t_{m1}}{14}\int_{2.5}^{-11.5}\frac{s}{\exp(s)-1}\exp\left(\frac{18t_{m1}}{35}\left(\exp\left(-\frac{70}{9}\right)\right.\right.$$
$$\left.\left.-\exp\left(-\frac{25-10s}{18}\right)\right)+\frac{t_{m1}}{14}\left[\mathrm{Li}_2(\exp(x))\right.\right.$$
$$\left.\left.+x\ln(1-\exp(x))-\frac{1}{2}x^2\right]\Big|_{s}^{-11.5}\right)ds, \quad \text{(B1)}$$

Based on Eq. (B1), we present the estimations of t_{m1} by choosing different open probabilities value for $m^{dy}(t_{m1})$ in Table I.

TABLE I. Estimation of t_{m1}.

$m^{dy}(t_{m1})$	0.93	0.95	0.97
t_{m1}	0.57 ms	0.67 ms	0.92 ms

TABLE II. Estimation of t_{m2}.

$m^{dy}(t_{m2})$	0.15	0.1	0.05
t_{m2}	2.44 ms	3.00 ms	4.01 ms

Table I shows that the estimation of t_{m1} through Eq. (B1) has consistent results. In the similar way, for the second time interval parameter t_{m2}, by substituting Eq. (36), Eq. (40) into Eq. (37), we obtain

$$m^{dy}(t_{m2}) = m_0 \exp\left(\frac{36t_{m2}}{75}\left(\exp\left(\frac{-70}{9}\right)-\exp\left(\frac{5}{9}\right)\right)\right.$$
$$+\frac{t_{m2}}{15}\left[\mathrm{Li}_2(\exp(x))+x\ln(1-\exp(x))-\frac{1}{2}x^2\right]\Big|_{3.5}^{-11.5}\Big)$$
$$+\frac{t_{m2}}{15}\int_{-11.5}^{3.5}\frac{s}{\exp(s)-1}\exp\left(\frac{36t_{m2}}{75}\left(\exp\left(\frac{-(35-10s)}{18}\right)\right.\right.$$
$$\left.\left.-\exp\left(\frac{5}{9}\right)\right)+\frac{t_{m2}}{15}\left[\mathrm{Li}_2(\exp(x))+x\ln(1-\exp(x))\right.\right.$$
$$\left.\left.-\frac{1}{2}x^2\right]\Big|_{3.5}^{s}\right)ds. \quad \text{(B2)}$$

In the second time interval, we choose $m^{dy}(t_{m1}) = 0.95$ as the initial value m_0 in Eq. (B2). Table II shows the consistent estimation of the t_{m2} when different value for $m^{dy}(t_{m2})$ has been chosen.

In sum, based on the results in Tables I and II, we confirm that by using Eqs. (B1) and (B2) to estimate the time parameter t_{m1} and t_{m2} for ΔV_{ax} have robust results.

APPENDIX C: ESTIMATION OF TRANSMEMBRANE CURRENTS

After the axon stop firing, we assume that voltage-gated Na^+ and K^+ channel's conductance on axon membrane have returned to their resting state in the stimulated region,

$$g_{ax}^{i,dy} \approx g_{ax}^{i,re}, \quad i = Na^+, K^+.$$

At this stage, we have ion channel conductance on the glial and axon membrane as

$$\{g_{ax}^{Na,re}, g_{ax}^{K,re}, g_{ax}^{Cl}, g_{gl}^{Cl}, g_{gl}^{Na}\} \subset o\left(g_{gl}^{K}\right). \quad \text{(C1)}$$

Similar to Eq. (53), we claim in the stimulated region,

$$\Delta E_k^i = o\left(\Delta E_{gl}^K\right), \quad i = Na^+, Cl^-, \quad k = gl, ax, \quad \text{(C2)}$$

since Eq. (57) and

$$c_{ex}^{K,re} = o\left(c_{ex}^{i,re}\right), \quad i = Na^+, Cl^-.$$

In addition, for the increase current through Na/K pump in Eq. (54), we have

$$z^{Na}e\Delta J_{p,k}^{Na} + z^{K}e\Delta J_{p,k}^{K} = \Delta I_k, \quad k = gl, ax.$$

By the Taylor expansion, we approximate the increase current through the Na/K pump due to the extracellular K^+ concentration changes as

$$\Delta I_k \approx 2\left(\frac{K_{K1}I_k^{re,1}}{c_{ex}^{K,re}(c_{ex}^{K,re}+K_{K1})}+\frac{K_{K2}I_k^{re,2}}{c_{ex}^{K,re}(c_{ex}^{K,re}+K_{K2})}\right)\Delta c_{ex}^K, \tag{C3}$$

where $I_k^{re,1}$ and $I_k^{re,2}$ are the resting state current through α_1- and α_2- isoform of the Na/K pump on glial membrane ($k=gl$) or axon membrane ($k=ax$).

By comparison between Eqs. (53) and (C3), we have

$$\Delta I_k = o\left(g_{gl}^K \Delta E_{gl}^K\right), \quad k=gl,ax. \tag{C4}$$

In all, based on the estimations in Eqs. (C1), (C2), and (C4), we claim the dominated term in the right-hand side of Eq. (54) is

$$\sum_i z^i e \mathscr{M}_{gl}\left(J_{p,gl}^i + J_{c,gl}^i\right) + \sum_i z^i e \mathscr{M}_{ax}\left(J_{p,ax}^i + J_{c,ax}^i\right) \approx \mathscr{M}_{gl} g_{gl}^K \left(\Delta V_{gl} - \Delta E_{gl}^K\right),$$

where we use the fact that at the resting state, the transmembrane currents in both axon membrane and glial membrane are negligible in comparison to the source term $g_{gl}^K \Delta E_{gl}^K$.

APPENDIX D: COMPARISON BETWEEN $\Delta\phi_{gl}$ AND $\Delta\phi_{ex}$

In this section, we show that the scale of the glial electric potential variation $\Delta\phi_{gl}$ is much larger than the scale of the extracellular electric variation $\Delta\phi_{ex}$ in the stimulated region. Based on Eq. (63), we know

$$O\left(\frac{\eta_{gl}\sigma_{gl}}{\eta_{ex}\sigma_{ex}}\right) = 10^{-2}, \quad O\left(\frac{\tau_{ex}eD_{ex}^{\text{diff}}}{\sigma_{ex}}\Delta c_{sti}\right) = 10^{-6}. \tag{D1}$$

If the $\Delta\phi_{ex} \neq o(\Delta\phi_{gl})$, then based on Eqs. (63) and (D1), we should have

$$O(\Delta\phi_{gl}) < 10^{-5}.$$

Therefore, the right-hand side of Eq. (62) becomes

$$\left|\frac{g_{gl}^K}{e}\left(\Delta V_{gl} - \Delta E_{gl}^K\right)\right| \approx \left|\frac{g_{gl}^K}{e}\Delta E_{gl}^K\right| = O(10^{-8}). \tag{D2}$$

where we use the estimation of $\Delta E_{gl}^K\,(=O(10^{-3}))$ in Eqs. (53) and (50), and

$$O(\Delta V_{gl}) = O(\Delta\phi_{gl} - \Delta\phi_{ex}) < 10^{-5}.$$

At the same time, the left-hand side of Eq. (62) gives

$$\left|\frac{2}{r_{sti}}\frac{\eta_{gl}\sigma_{gl}}{\mathscr{M}_{gl}}\frac{\Delta\phi_{gl}}{r^*}\right| < O(10^{-11}). \tag{D3}$$

In Eq. (62), based on Eqs. (D3) and (D2), the order of the right-hand side does not match with the order of the left-hand side. Therefore, we conclude that

$$\Delta\phi_{ex} = o(\Delta\phi_{gl}).$$

APPENDIX E: ESTIMATION OF EXTRACELLULAR Na^+ AND K^+ TRANSPORT

For the K^+ clearance in the stimulated extracellular region in Eq. (72), based on Eqs. (53) and (67), the effect of average glial transmembrane K^+ flux in the stimulated region is

$$\lambda_{gl}^{m,K} = \frac{\mathscr{M}_{gl} g_{gl}^K h_\varepsilon k_B T}{z^K(1+h_\varepsilon)e^2 c_{ex}^{K,re}}. \tag{E1}$$

For K^+ flux through the extracellular pathway, we only consider the effects from diffusion and electric drift terms in the radial K^+ flux. The fluid flows in the extracellular space from the non-stimulated region to the stimulated region. So, the convection flux in the extracellular is a consequence of the osmosis and flattens the variation of osmotic pressure in the stimulated region.

The scale of the radial diffusive K^+ flux in the extracellular space can be approximated as

$$O\left(-D_{ex}^K \tau_{ex}\frac{dc_{ex}^K}{dr}\right) = \frac{D_{ex}^K\tau_{ex}}{r^*}\Delta c_{ex}^K. \tag{E2}$$

The scale of the radial electric drift K^+ flux in the extracellular space is

$$O\left(-\frac{D_{ex}^K\tau_{ex}e}{k_BT}c_{ex}^K\frac{d\phi_{ex}}{dr}\right) = \frac{D_{ex}^K\tau_{ex}e}{k_BT}c_{ex}^K\frac{\Delta\phi_{ex}}{r^*} \approx -\frac{\eta_{gl}\sigma_{gl}D_{ex}^K\tau_{ex}}{\eta_{ex}\sigma_{ex}(1+h_\varepsilon)r^*}\Delta c_{ex}^K, \tag{E3}$$

where $\Delta\phi_{ex}$ used the estimation from Eq. (68).

Based on Eqs. (E2) and (E3), we note that the electric drift K^+ flux is in the opposite radial direction to the diffusive K^+ flux in the extracellular space. At the same time, the electric drift K^+ flux has a much smaller magnitude than the diffusive K^+ flux because the ratio R_{ex}^K between the electric drift and diffusion terms is

$$R_{ex}^K = \frac{\eta_{gl}\sigma_{gl}}{\eta_{ex}\sigma_{ex}(1+h_\varepsilon)} = o(1). \tag{E4}$$

Therefore, in Eq. (72), the average effect of the K^+ transport through extracellular pathway can be approximated as

$$\lambda_{ex}^K = \frac{2\eta_{ex}D_{ex}^K\tau_{ex}}{r_{sti}r^*}, \tag{E5}$$

where we used the ratio between volume V_S and the effective radial surface.

In Eq. (73), we first look for the effect of Na^+ fluxes through the extracellular pathway. Similar to Eq. (E2), the scale of the radial diffusive Na^+ flux in the extracellular space is

$$O\left(-D_{ex}^{Na}\tau_{ex}\frac{dc_{ex}^{Na}}{dr}\right) = \frac{D_{ex}^{Na}\tau_{ex}}{r^*}\Delta c_{ex}^{Na}. \tag{E6}$$

The scale of the radial electric drift flux for Na^+ in in the extracellular space is

$$O\left(-\frac{D_{ex}^{Na}\tau_{ex}e}{k_BT}c_{ex}^{Na}\frac{d\phi_{ex}}{dr}\right)=\frac{D_{ex}^{Na}\tau_{ex}e}{k_BT}c_{ex}^{Na}\frac{\Delta\phi_{ex}}{r^*}$$
$$\approx-\frac{\eta_{gl}\sigma_{gl}D_{ex}^{Na}\tau_{ex}}{\eta_{ex}\sigma_{ex}(1+h_\varepsilon)r^*}\frac{c_{ex}^{Na}}{c_{ex}^{K}}\Delta c_{ex}^{K} \quad \text{(E7)}$$

For Na^+ in the extracellular space, the radial electric drift Na^+ flux is in the same direction as the radial diffusive K^+ flux since Δc_{ex}^{Na} is negative in the stimulated region.

The scale of the radial diffusive Na^+ flux is at the same level as the radial electric drift Na^+ flux in the extracellular space. From Eqs. (E6) and (E7), the ratio R_{ex}^{Na} is

$$R_{ex}^{Na}=\frac{\eta_{gl}\sigma_{gl}}{\eta_{ex}\sigma_{ex}(1+h_\varepsilon)}\frac{c_{ex}^{Na}}{c_{ex}^{K}}=O(1), \quad \text{(E8)}$$

since Δc_{ex}^{Na} and Δc_{ex}^{K} is at the same leading order. The Na^+ flux through glial transmembrane is much smaller than the K^+ flux such that

$$\lambda_{gl}^{m,Na}=o\left(\lambda_{gl}^{m,K}\right). \quad \text{(E9)}$$

This is because of the conductance on the glial membrane $g_{gl}^{Na}=o(g_{gl}^{K})$. The effect of Na^+ flux through glial transmembrane can be neglected in Eq. (73), since Eq. (E9), and the diffusive fluxes in Eqs. (E6) and (E2) are in the same magnitude. In sum, for Eq. (73), we get

$$\lambda_{ex}^{Na,1}=\frac{2\eta_{ex}D_{ex}^{Na}\tau_{ex}}{r_{sti}r^*}, \quad \lambda_{ex}^{Na,2}=\frac{2\eta_{gl}\sigma_{gl}D_{ex}^{Na}\tau_{ex}c_{ex}^{Na,re}}{r_{sti}\sigma_{ex}(1+h_\varepsilon)r^*c_{ex}^{K,re}}.$$

where we used the ratio between volume V_S and the effective radial surface.

In the end of this section, we consider the solution for the coupled dynamical system of (72) and (73)

$$\frac{d}{dt}\begin{pmatrix}\Delta c_{ex}^{K}\\ \Delta c_{ex}^{Na}\end{pmatrix}=A\begin{pmatrix}\Delta c_{ex}^{K}\\ \Delta c_{ex}^{Na}\end{pmatrix}, \quad \text{(E10)}$$

where

$$A=\begin{bmatrix}A_{11}&0\\A_{21}&A_{22}\end{bmatrix}=\begin{bmatrix}-\left(\lambda_{gl}^{m,K}+\lambda_{ex}^{K}\right)/\eta_{ex}^{re}&0\\ \lambda_{ex}^{Na,2}/\eta_{ex}^{re}&-\lambda_{ex}^{Na,1}/\eta_{ex}^{re}\end{bmatrix}. \quad \text{(E11)}$$

In the system (E10), we assume that η_{ex} keeps at its resting state (η_{ex}^{re}) and the initial condition is

$$\begin{pmatrix}\Delta c_{ex}^{K,0}\\ \Delta c_{ex}^{Na,0}\end{pmatrix}=\begin{pmatrix}\Delta c_{sti}\\ -\Delta c_{sti}\end{pmatrix}. \quad \text{(E12)}$$

The solution for system (E10) in the time interval $t\in[0,T]$ is

$$\begin{cases}\Delta c_{ex}^{K}(t)=\Delta c_{sti}\exp(A_{11}t),\\ \Delta c_{ex}^{Na}(t)=\dfrac{A_{21}\Delta c_{sti}}{A_{11}-A_{22}}(\exp(A_{11}t)-\exp(A_{22}t))-\Delta c_{sti}\exp(A_{22}t),\end{cases} \quad \text{(E13)}$$

where T is the time interval between each single action potential in the axon compartment. There are $n\left(=\frac{T_{sti}}{f_m}\right)$ stimuli in the time interval $[0,T_{sti}=nT]$, we have

$$\Delta c_{ex}^{K}(iT)=\Delta c_{ex}^{K}(iT)+\Delta c_{sti},\ \Delta c_{ex}^{Na}(iT)=\Delta c_{ex}^{Na}(iT)-\Delta c_{sti}.$$
$$i=1\ldots n-1,$$

In the above, we view the extracellular K^+ and Na^+ concentration immediately changes due to axon firing. By using Eq. (E13), we have

$$\Delta c_{ex}^{K}(nT)=\Delta c_{sti}\frac{\exp(A_{11}T)-\exp((n+1)A_{11}T)}{1-\exp(A_{11}T)}, \quad \text{(E14)}$$

and

$$\Delta c_{ex}^{Na}(nT)=\sum_{i=1}^{n}\frac{A_{21}\Delta c_{ex}^{K}((i-1)T)}{4}(\exp(A_{11}T)-\exp(A_{22}T))$$
$$\times\exp((n-i)A_{22}T)-\Delta c_{sti}\sum_{i=1}^{n}\exp(iA_{22}T), \quad \text{(E15)}$$

where

$$\Delta c_{ex}^{K}(jT)=\Delta c_{sti}\frac{1-\exp((j+1)A_{11}T)}{1-\exp(A_{11}T)}, \quad j=0,1,\ldots n-1.$$

APPENDIX F: SPATIAL DISTRIBUTION OF VELOCITY AND OSMOTIC PRESSURE

Figure 16 shows longitudinal direction changes of volume fractions of extracellular space and glial compartment at $r=1.5\,\mu m$.

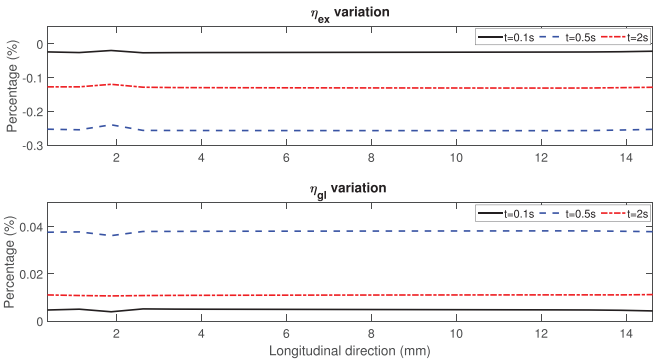

FIG. 16. Longitudinal direction changes of η_{ex} and η_{gl} at $r=1.5\mu m$ at $t=0.1s, 0.5s, 2s$.

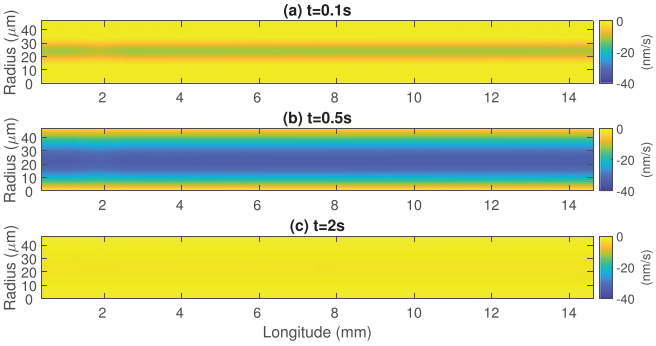

FIG. 17. Spatial distribution of velocity in radius direction during and after a train of stimuli.

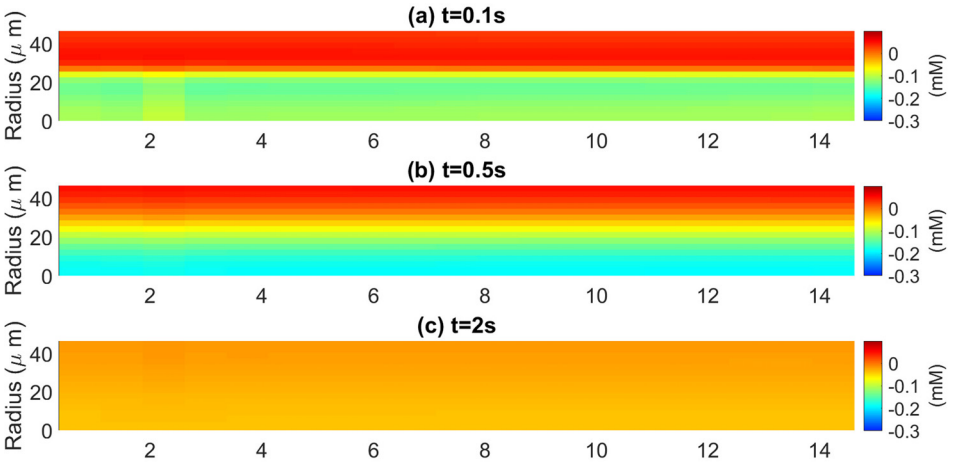

FIG. 18. Spatial distribution of osmotic pressure changes from resting state during and after a train of stimuli.

TABLE III. Parameters in optic nerve model.

Parameters	Value	Parameters	Value
R_a	4.8×10^{-5} m (Refs. 16 and 75)	μ	7×10^{-4} Pa s (Ref. 76)
R_b	6×10^{-5}m (Ref. 77)	$c^{Na}_{csf,eye}$	111 mM (Ref. 16)
L	1.5×10^{-2} m (Ref. 16)	$c^{K}_{csf,eye}$	3 mM (Ref. 16)
e	1.69×10^{-19} A s	$c^{Na,re}_{gl}$	7.57 mM[a]
k_B	1.38×10^{-23} J/K	$c^{K,re}_{gl}$	100.84 mM[a] (Ref. 16)
T	296.15 K (Ref. 16)	$c^{Na,re}_{ax}$	10.17 mM[a]
η^{re}_{ax}	5×10^{-1} (Ref. 16)	$c^{K,re}_{ax}$	100.04 mM[a]
η^{re}_{gl}	4×10^{-1} (Ref. 16)	$A^{re}_{ax,gl}$	105 mM[a]
η^{re}_{ex}	1×10^{-1} (Ref. 16)	τ^{OP}_{ex}	0.16 (Refs. 51 and 76)
$\mathscr{M}_{ax}$	5.9×10^{6} m^{-1} (Ref. 78)	τ^{SAS}_{ex}	1[a]
$\mathscr{M}_{gl}$	1.25×10^{7} m^{-1} (Ref. 78)	τ_{gl}	0.5[a]
$z^{Na,K}$	1	p_{CSF}	1.3×10^{3} Pa (Ref. 57)
z^{Cl}	−1	p_{ICP}	4×10^{3} Pa (Ref. 57)
$z^{ax,gl}$	−1[a]	p_{OBP}	0 Pa (Ref. 57)
$\gamma_{ax,gl}$	1 (Refs. 51 and 76)	$D^{Na}_{ex,ax}$	1.39×10^{-9} m^2/s (Ref. 76)
γ_{pia}	1 (Refs. 51 and 76)	$D^{K}_{ex,ax}$	2.04×10^{-9} m^2/s (Ref. 76)
$K_{Na1,Na2}$	2.339 3 mM (Ref. 46)	$D^{Cl}_{ex,ax}$	2.12×10^{-9} m^2/s (Ref. 76)
K_{K1}	1.615 4 mM (Ref. 46)	D^{Na}_{gl}	1.39×10^{-11} m^2/s (Ref. 76)
K_{K2}	0.165 7 mM (Ref. 46)	D^{K}_{gl}	2.04×10^{-11} m^2/s (Ref. 76)
$I_{gl,1}$	4.78×10^{-4} A/m^{2,b} (Ref. 46)	D^{Cl}_{gl}	2.12×10^{-11} m^2/s (Ref. 76)
$I_{gl,2}$	6.5×10^{-5} A/m^{2,b} (Ref. 46)	k^{OP}_{ex}	$1.372\,9 \times 10^{-8}$ m^2/ · s (Ref. 51)
$I_{ax,1}$	9.56×10^{-4} A/m^{2,b} (Ref. 46)	k^{SAS}_{ex}	0 m^2/V · s[a]
$I_{ax,2}$	1.3×10^{-4} A/m^{2,b} (Ref. 46)	K_{ax}	1.67×10^{6} Pa (Refs. 22 and 79)
g^{Na}_{gl}	2.2×10^{-3} S/m^2 (Ref. 76)	K_{gl}	8.33×10^{5} Pa (Refs. 22 and 79)
g^{K}_{gl}	2.1 S/m^2 (Ref. 76)	L^{m}_{dr}	8.89×10^{-13} m/Pa s (Refs. 46 and 51)
g^{Cl}_{gl}	2.2×10^{-3} S/m^2 (Ref. 76)	L^{m}_{pia}	8.89×10^{-13} m/Pa s (Refs. 46 and 51)
g^{Na}_{leak}	4.8×10^{-3} S/m^{2,b} (Ref. 80)	L^{m}_{gl}	1.34×10^{-13} m/Pa s (Refs. 46 and 51)
g^{K}_{leak}	2.2×10^{-2} S/m^{2,b} (Ref. 80)	L^{m}_{ax}	7.954×10^{-14} m/Pa s (Ref. 81)

TABLE III. (*Continued.*)

Parameters	Value	Parameters	Value
$\bar{g}^{Na}$	1.357×10^{1} S/m^{2,b} (Ref. 80)	κ_{gl}	9.366×10^{-19} m^2 (Refs. 46 and 51)
$\bar{g}^{K}$	2.945 S/m^{2,b} (Ref. 80)	κ_{ax}	1.33×10^{-16} m^2 (Refs. 46 and 51)
g_{ax}^{Cl}	1.5×10^{-1} S/m^{2,a}	κ_{ex}^{OP}	3.99×10^{-16} m^{2,b} (Refs. 46 and 51)
$G_{pia}^{Na,K,Cl}$	3 S/m^{2,a}	κ_{ex}^{SAS}	1.33×10^{-14} m^{2,b} (Refs. 46 and 51)

[a]Estimated or induced from the concentration balance.
[b]Deducted proportionally from reference.

Figure 17 shows the spatial distribution of velocity in radius direction during and after a train of stimuli. Figure 18 shows the spatial distribution of osmotic pressure changes from resting state during and after a train of stimuli. Table III shows all values of parameters used in the simulations.

DATA AVAILABILITY

The data that support the findings of this study are available from the corresponding authors upon reasonable request.

REFERENCES

[1]W. M. Gelbart and A. Ben-Shaul, "The 'new' science of 'complex fluids,'" J. Phys. Chem. **100**, 13169–13189 (1996).
[2]J. M. Krishnan, A. P. Deshpande, and P. S. Kumar, *Rheology of Complex Fluids* (Springer, 2010).
[3]S. E. Spagnolie, *Complex Fluids in Biological Systems*, Biological and Medical Physics, Biomedical Engineering (Springer, 2015).
[4]G. G. Fuller and J. Vermant, "Complex fluid-fluid interfaces: Rheology and structure," Annu. Rev. Chem. Biomol. Eng. **3**, 519–543 (2012).
[5]B. Eisenberg, Y. Hyon, and C. Liu, "Energy variational analysis of ions in water and channels: Field theory for primitive models of complex ionic fluids," J. Chem. Phys. **133**, 104104 (2010).
[6]E. R. Kandel, J. H. Schwartz, T. M. Jessell, S. Siegelbaum, A. J. Hudspeth, and S. Mack, *Principles of Neural Science* (McGraw-Hill, New York, 2000), Vol. 4.
[7]J. G. Nicholls, A. R. Martin, B. G. Wallace, and P. A. Fuchs, *From Neuron to Brain* (Sinauer Associates, Sunderland, MA, 2001), Vol. 271.
[8]W. F. Boron and E. L. Boulpaep, *Medical Physiology E-Book* (Elsevier Health Sciences, 2016).
[9]M. Nedergaard and S. A. Goldman, "Glymphatic failure as a final common pathway to dementia," Science **370**, 50–56 (2020).
[10]R. Orkand, J. Nicholls, and S. Kuffler, "Effect of nerve impulses on the membrane potential of glial cells in the central nervous system of amphibia," J. Neurophysiol. **29**, 788–806 (1966).
[11]B. Frankenhaeuser and A. Hodgkin, "The after-effects of impulses in the giant nerve fibres of loligo," J. Physiol. **131**, 341–376 (1956).
[12]J. J. Salazar, A. I. Ramírez, R. De Hoz, E. Salobrar-Garcia, P. Rojas, J. A. Fernández-Albarral, I. López-Cuenca, B. Rojas, A. Triviño, and J. M. Ramírez, "Anatomy of the human optic nerve: Structure and function," *Optic Nerve* (IntechOpen, 2018).
[13]J. B. Selhorst and Y. Chen, "The optic nerve," in *Seminars in Neurology* (Thieme Medical Publishers, 2009), Vol. 29, pp. 29–35.
[14]S. S. Hayreh, "Ischemic optic neuropathy," Prog. Retinal Eye Res. **28**, 34–62 (2009).
[15]D. A. Atchison, G. Smith, and G. Smith, *Optics of the Human Eye* (Butterworth-Heinemann, Oxford, 2000), Vol. 2.
[16]S. Kuffler, J. Nicholls, and R. Orkand, "Physiological properties of glial cells in the central nervous system of amphibia," J. Neurophysiol. **29**, 768–787 (1966).
[17]A. Bellot-Saez, O. Kekesi, J. W. Morley, and Y. Buskila, "Astrocytic modulation of neuronal excitability through k+ spatial buffering," Neurosci. Biobehavioral Rev. **77**, 87–97 (2017).
[18]A. Wallraff, R. Köhling, U. Heinemann, M. Theis, K. Willecke, and C. Steinhäuser, "The impact of astrocytic gap junctional coupling on potassium buffering in the hippocampus," J. Neurosci. **26**, 5438–5447 (2006).
[19]S. S. Hayreh, "The sheath of the optic nerve," Ophthalmologica **189**, 54–63 (1984).
[20]H. Killer, H. Laeng, J. Flammer, and P. Groscurth, "Architecture of arachnoid trabeculae, pillars, and septa in the subarachnoid space of the human optic nerve: Anatomy and clinical considerations," Br. J. Ophthalmol. **87**, 777–781 (2003).
[21]M. Pache and P. Meyer, "Morphological changes of the retrobulbar optic nerve and its meningeal sheaths in glaucoma," Ophthalmologica **220**, 393–396 (2006).
[22]Y. Hua, A. P. Voorhees, and I. A. Sigal, "Cerebrospinal fluid pressure: Revisiting factors influencing optic nerve head biomechanics," Invest. Ophthalmol. Visual Sci. **59**, 154–165 (2018).
[23]K. Andres, M. V. Düring, K. Muszynski, and R. Schmidt, "Nerve fibres and their terminals of the dura mater encephali of the rat," Anat. Embryol. **175**, 289–301 (1987).
[24]H. E. Killer, H. R. Laeng, and P. Groscurth, "Lymphatic capillaries in the meninges of the human optic nerve," J. Neuro-ophthalmol. **19**, 222–228 (1999).
[25]W. H. Morgan, C. Balaratnasingam, C. R. Lind, S. Colley, M. H. Kang, P. H. House, and D.-Y. Yu, "Cerebrospinal fluid pressure and the eye," Br. J. Ophthalmol. **100**, 71–77 (2016).
[26]A. S. Filippidis, S. G. Zarogiannis, M. Ioannou, K. Gourgoulianis, P.-A. Molyvdas, and C. Hatzoglou, "Permeability of the arachnoid and pia mater. the role of ion channels in the leptomeningeal physiology," Child's Nervous Syst. **28**, 533–540 (2012).
[27]K. Vogiatzidis, C. Hatzoglou, S. Zarogiannis, G. Matafia, K. Gourgoulianis, and P.-A. Molyvdas, "μ-opioid influence on transmesothelial resistance of isolated sheep pleura and parietal pericardium," Eur. J. Pharmacol. **530**, 276–280 (2006).
[28]C. Hatzoglou, K. Gourgoulianis, and P. Molyvdas, "Effects of snp, ouabain, and amiloride on electrical potential profile of isolated sheep pleura," J. Appl. Physiol. **90**, 1565–1569 (2001).
[29]D. K. Payne, G. T. Kinasewitz, and E. Gonzalez, "Comparative permeability of canine visceral and parietal pleura," J. Appl. Physiol. **65**, 2558–2564 (1988).
[30]S. Sarkos, C. Hatzoglou, J. Dahabre, K. Gourgoulianis, and P. Molyvdas, "Effect of amiloride in human and sheep parietal pleura," Respir. Physiol. Neurobiol. **132**, 233–237 (2002).
[31]S. Zarogiannis, C. Hatzoglou, I. Stefanidis, M. Ioannou, E. Paraskeva, K. Gourgoulianis, and P.-A. Molyvdas, "Comparison of the electrophysiological properties of the sheep isolated costal and diaphragmatic parietal pleura," Clin. Exp. Pharmacol. Physiol. **34**, 129–131 (2007).
[32]S. Zarogiannis, C. Hatzoglou, I. Stefanidis, V. Liakopoulos, K. Gourgoulianis, and P.-A. Molyvdas, "Adrenergic influence on the permeability of sheep diaphragmatic parietal pleura," Respiration **74**, 118–120 (2007).
[33]S. Zarogiannis, T. Deligiorgi, I. Stefanidis, V. Liakopoulos, K. Gourgoulianis, P. A. Molyvdas, and C. Hatzoglou, "Dexamethasone decreases the transmesothelial electrical resistance of the parietal and visceral pleura," J. Physiol. Sci. **59**, 335–339 (2009).

[34]F. K. Li, C. H. To, J. Leung, T. M. Chan, and K. N. Lai, "Electrophysiology and glucose transport of human peritoneal mesothelial cells: Implications for peritoneal dialysis," Peritoneal Dial. Int. **21**, 115–121 (2001).
[35]M. Simon, "Peritoneal mesothelium in vitro: An electrophysiologic study," Peritoneal Dial. Int. **16**, 393–397 (1996).
[36]I. Stefanidis, V. Liakopoulos, P. Kourti, S. Zarogiannis, A. Poultsidi, P. R. Mertems, M. Salmas, C. Hatzoglou, K. Gourgoulianis, and P.-A. Molyvdas, "Amiloride-sensitive sodium channels on the parietal human peritoneum: Evidence by ussing-type chamber experiments," Asaio J. **53**, 335–338 (2007).
[37]S. Zarogiannis, P. Kourti, C. Hatzoglou, V. Liakopoulos, A. Poultsidi, K. Gourgoulianis, P. Molyvdas, and I. Stefanidis, "Influence of the sodium transport inhibition by amiloride on the transmesothelial resistance of isolated visceral sheep peritoneum." Adv. Peritoneal Dial. **21**, 5–8 (2005).
[38]S. Zarogiannis, V. Liakopoulos, C. Hatzoglou, P. Kourti, K. Vogiatzidis, S. Potamianos, T. Eleftheriadis, K. Gourgoulianis, P. Molyvdas, and I. Stefanidis, "Effect of sodium-potassium pump inhibition by ouabain on the permeability of isolated visceral sheep peritoneum," Adv. Peritoneal Dial. **23**, 43–47 (2007).
[39]S. Zarogiannis, K. Vogiatzidis, C. Hatzoglou, V. Liakopoulos, S. Potamianos, T. Eleftheriadis *et al.*, "μ-opioid stimulation of isolated parietal sheep peritoneum decreases peritoneal permeability in vitro," Adv. Peritoneal Dial. **23**, 34–37 (2007).
[40]C. Verikouki, C. Hatzoglou, K. Gourgoulianis, P. Molyvdas, A. Kallitsaris, and I. Messinis, "Rapid effect of progesterone on transepithelial resistance of human fetal membranes: Evidence for non-genomic action," Clin. Exp. Pharmacol. Physiol. **35**, 174–179 (2008).
[41]E. A. Adams, H. M. Choi, C. Y. Cheung, and R. A. Brace, "Comparison of amniotic and intramembranous unidirectional permeabilities in late-gestation sheep," Am. J. Obstetr. Gynecol. **193**, 247–255 (2005).
[42]A. Filippidis, S. Zarogiannis, M. Ioannou, K. Gourgoulianis, P.-A. Molyvdas, and C. Hatzoglou, "Transmembrane resistance and histology of isolated sheep leptomeninges," Neurol. Res. **32**, 205–208 (2010).
[43]Y. Zhu, S. Xu, R. S. Eisenberg, and H. Huang, "A tridomain model for potassium clearance in optic nerve," arXiv:2012.03303 (2020).
[44]C. Nicholson, "Diffusion and related transport mechanisms in brain tissue," Rep. Progress Phys. **64**, 815 (2001).
[45]S. Xu, B. Eisenberg, Z. Song, and H. Huang, "Osmosis through a semipermeable membrane: A consistent approach to interactions," arXiv:1806.00646 (2018).
[46]Y. Zhu, S. Xu, R. S. Eisenberg, and H. Huang, "A bidomain model for lens microcirculation," Biophys. J. **116**, 1171–1184 (2019).
[47]Y. Mori, "A multidomain model for ionic electrodiffusion and osmosis with an application to cortical spreading depression," Physica D **308**, 94–108 (2015).
[48]S. Xu, P. Sheng, and C. Liu, "An energetic variational approach for ion transport," Commun. Math. Sci. **12**, 779–789 (2014).
[49]G. Allaire, A. Mikelić, and A. Piatnitski, "Homogenization of the linearized ionic transport equations in rigid periodic porous media," J. Math. Phys. **51**, 123103 (2010).
[50]N. Ray, T. van Noorden, F. Frank, and P. Knabner, "Multiscale modeling of colloid and fluid dynamics in porous media including an evolving microstructure," Transp. Porous Media **95**, 669–696 (2012).
[51]D. T. K. Malcolm, "A computational model of the ocular lens," Ph.D. thesis (ResearchSpace, Auckland, 2006).
[52]G. B. Benedek and F. M. Villars, *Physics with Illustrative Examples from Medicine and Biology: Mechanics* (Springer Science & Business Media, 2000).
[53]M. Pérez-Pinzón, L. Tao, and C. Nicholson, "Extracellular potassium, volume fraction, and tortuosity in rat hippocampal ca1, ca3, and cortical slices during ischemia," J. Neurophysiology **74**, 565–573 (1995).
[54]S. McLaughlin and R. T. Mathias, "Electro-osmosis and the reabsorption of fluid in renal proximal tubules," J. Gen. Physiol. **85**, 699–728 (1985).
[55]E. Vaghefi, D. T. Malcolm, M. D. Jacobs, and P. J. Donaldson, "Development of a 3d finite element model of lens microcirculation," Biomed. Eng. Online **11**, 69 (2012).
[56]L. Wan, S. Xu, M. Liao, C. Liu, and P. Sheng, "Self-consistent approach to global charge neutrality in electrokinetics: A surface potential trap model," Phys. Rev. X **4**, 011042 (2014).
[57]L. R. Band, C. L. Hall, G. Richardson, O. E. Jensen, J. H. Siggers, and A. J. Foss, "Intracellular flow in optic nerve axons: A mechanism for cell death in glaucoma," Invest. Ophthalmol. Visual Sci. **50**, 3750–3758 (2009).
[58]R. E. Norman, J. G. Flanagan, I. A. Sigal, S. M. Rausch, I. Tertinegg, and C. R. Ethier, "Finite element modeling of the human sclera: Influence on optic nerve head biomechanics and connections with glaucoma," Exp. Eye Res. **93**, 4–12 (2011).
[59]B. S. Gardiner, D. W. Smith, M. Coote, and J. G. Crowston, "Computational modeling of fluid flow and intra-ocular pressure following glaucoma surgery," PLoS One **5**, e13178 (2010).
[60]R. Fitzhugh, "Thresholds and plateaus in the hodgkin–huxley nerve equations," J. Gen. Physiol. **43**, 867–896 (1960).
[61]F. Gabbiani and S. J. Cox, *Mathematics for Neuroscientists* (Academic Press, 2017).
[62]J. Gao, X. Sun, V. Yatsula, R. Wymore, and R. Mathias, "Isoform-specific function and distribution of na/k pumps in the frog lens epithelium," J. Membr. Biol. **178**, 89–101 (2000).
[63]K. Susuki, "Myelin: A specialized membrane for cell communication," Nat. Educ. **3**, 59 (2010).
[64]I. Ø stby, L. Øyehaug, G. T. Einevoll, E. A. Nagelhus, E. Plahte, T. Zeuthen, C. M. Lloyd, O. P. Ottersen, and S. W. Omholt, "Astrocytic mechanisms explaining neural-activity-induced shrinkage of extraneuronal space," PLoS Comput. Biol. **5**, e1000272 (2009).
[65]R. Keynes, "The ionic movements during nervous activity," J. Physiol. **114**, 119 (1951).
[66]I. Dietzel, U. Heinemann, G. Hofmeier, and H. Lux, "Stimulus-induced changes in extracellular na+ and cl- concentration in relation to changes in the size of the extracellular space," Exp. Brain Res. **46**, 73–84 (1982).
[67]J. M. Smith, D. P. Bradley, M. F. James, and C. L.-H. Huang, "Physiological studies of cortical spreading depression," Biol. Rev. **81**, 457–481 (2006).
[68]J. P. Dreier and C. Reiffurth, "The stroke-migraine depolarization continuum," Neuron **86**, 902–922 (2015).
[69]K. C. Chen and C. Nicholson, "Spatial buffering of potassium ions in brain extracellular space," Biophys. J. **78**, 2776–2797 (2000).
[70]S. Murakami and Y. Kurachi, "Mechanisms of astrocytic k+ clearance and swelling under high extracellular k+ concentrations," J. Physiol, Sci. **66**, 127–142 (2016).
[71]M. J. Sætra, G. Halnes, and G. T. Einevoll, "An electrodiffusive neuron-extracellular-glia model with somatodendritic interactions," bioRxiv (2020).
[72]K. Holthoff and O. W. Witte, "Directed spatial potassium redistribution in rat neocortex," Glia **29**, 288–292 (2000).
[73]P. Kofuji and E. A. Newman, "Potassium buffering in the central nervous system," Neuroscience **129**, 1043–1054 (2004).
[74]S. Chiu, J. Ritchie, R. Rogart, and D. Stagg, "A quantitative description of membrane currents in rabbit myelinated nerve," J. Physiol. **292**, 149–166 (1979).
[75]H. Bracho, P. Orkand, and R. Orkand, "A further study of the fine structure and membrane properties of neuroglia in the optic nerve of necturus," J. Neurobiol. **6**, 395–410 (1975).
[76]R. T. Mathias, "Steady-state voltages, ion fluxes, and volume regulation in syncytial tissues," Biophys. J. **48**, 435 (1985).
[77]N. Wang, *Intraocular and Intracranial Pressure Gradient in Glaucoma* (Springer, 2019), Vol. 1.
[78]C. Pilgrim, I. Reisert, and D. Grab, "Volume densities and specific surfaces of neuronal and glial tissue elements in the rat supraoptic nucleus," J. Comparative Neurology **211**, 427–431 (1982).
[79]Y.-B. Lu, K. Franze, G. Seifert, C. Steinhäuser, F. Kirchhoff, H. Wolburg, J. Guck, P. Janmey, E.-Q. Wei, J. Käs *et al.*, "Viscoelastic properties of individual glial cells and neurons in the CNS," Proc. Natl. Acad. Sci. **103**, 17759–17764 (2006).
[80]Z. Song, X. Cao, and H. Huang, "Electroneutral models for dynamic Poisson-Nernst-Planck systems," Phys. Rev. E **97**, 012411 (2018).
[81]R. Villegas and G. M. Villegas, "Characterization of the membranes in the giant nerve fiber of the squid," J. Gen. Physiol. **43**, 73 (1960).